

# Normal fault growth in layered basaltic rocks: the role of strain rate in fault evolution

A. Bubeck<sup>1</sup>, R.J. Walker<sup>1</sup>, J. Imber<sup>2</sup>, C.J. MacLeod<sup>3</sup>

<sup>1</sup>*School of Geography, Geology, and the Environment, University of Leicester, University Road, Leicester, UK.*

<sup>2</sup>*Department of Earth Sciences, Durham University, Science Labs, Durham, UK.*

<sup>3</sup>*School of Earth and Ocean Science, Cardiff University, Park Place, Cardiff, UK*

\*Correspondence ([ab753@le.ac.uk](mailto:ab753@le.ac.uk))

## ABSTRACT

Conceptual models for the evolution of dilatant faults in volcanic rift settings involve a step-wise growth pattern, involving upward propagation of subsurface faults, surface monocline formation, which are breached by subvertical, open faults. Immature, discontinuous normal faults are considered representative of the early stages of mature, linked faults that accommodate extensional strains. We consider the evolution of surface-breaking normal faults using a comparison of the distribution and geometry of normal faults from two volcanic rift zones: the Koa'e fault system, Hawai'i, and the Krafla fissure swarm, NE Iceland. Field mapping highlights similarities to current predicted geometries, but also prominent differences that are not reconciled by current models. Variable deformation styles record magma supply changes within the rift zones, which drive local strain rate gradients. Building on existing studies, we present a conceptual model of fault growth that accounts for spatial and temporal changes in strain rate within the deforming regions. We propose that faults in separate rift systems may not advance through the same stages of evolution and that faults within *individual* rift systems can show differing growth patterns. Variations in

surface strains may be indicative of subsurface magmatic system changes, with important implications for our understanding of volcano-tectonic coupling.

**Key words: normal fault; monocline; extension; basalt; volcanic rift**

## **1.1. Introduction**

Normal fault systems comprise discontinuous, non-collinear segments, with overlaps and segment linkage commonly resulting in characteristic overlapping or step-like geometries across a broad range of scales (e.g. Segall and Pollard, 1980; Peacock, 2002; Long and Imber, 2011). Regional extension is conserved ahead of first-order fault terminations by areas of folding and linking faults and fractures (e.g. Morley et al., 1990; Faulds and Varga, 1998). The geometry and distribution of structures within these domains play an important role in the tectono-stratigraphic development of rift basins (e.g. Lambiase and Bosworth, 1995; Sharp et al., 2000; Hus et al., 2006), and the evolving fluid flow properties of fault zones (e.g. Manzocchi et al., 2010; Seebeck et al., 2014). Much of our current understanding of the growth of normal fault populations and fault zone architecture is derived from studies of faults in clastic sequences using combinations of: (1) fault analysis and scaling relationships, based on field and seismic data-derived measurements of displacement and length versus width (e.g. Ferrill and Morris, 2001; Peacock, 2002; Walsh et al., 2003; Nixon et al., 2014); (2) scaled-analogue modelling (e.g. Holland et al., 2006; Tentler and Acocella, 2010); and (3) numerical-based modelling techniques (e.g. Crider and Pollard, 1998; Maerten et al., 2002; Schöpfer et al., 2006). Many of these studies have focussed on fault propagation and segmentation within layered clastic sequences (e.g. Ferrill and Morris, 2003), and more recently crystalline-clastic sequences (e.g. Peacock and Parfitt, 2002; Holland et al., 2006; Martel and Langley, 2006; Kaven and Martel, 2007; Walker et al., 2013). The growth of normal

faults in layered basaltic sequences, and the expression of those faults outcropping at surface, has become increasingly important in recent years, driven in part by interest in intra- and sub-volcanic hydrocarbon plays along volcanic passive margins (e.g., the NE Atlantic basins: Davison et al., 2004; Walker et al., 2012, 2013), as well as high-temperature shallow geothermal systems that rely on basaltic stratigraphy (e.g. Anderson and Bowers, 1995; Helm-Clark et al., 2004) and models of volcanic flank stability (e.g. Le Corvec and Walter, 2009; Plattner et al., 2013). An improved understanding of basalt-hosted fault zones has important implications for extension in continental and oceanic systems on Earth, as well as on other planets (e.g. Hauber et al., 2010; Vaz et al., 2014).

Existing models for the growth of normal faults in basaltic sequences typically depict development in a common series of static stages with the progression between stages treated as instantaneous (e.g. Martel and Langley, 2006). Emphasis is placed on the reactivation of pre-existing cooling joints through the entire layer sequence; considered to be the first-order control on the distribution, geometry and architecture of basalt-hosted fault zones (e.g. Forslund and Gudmundsson, 1992; Gudmundsson, 2011). A single growth process implies that small-displacement faults in immature or early-stage rift systems are also representative of faults in more advanced systems, with all faults progressing through the same stages of evolution. As such, models of fault growth in cohesive sequences are broadly applied to a wide range of settings.

Here, we present a detailed field study of the distribution and geometry of well-exposed extensional structures in two developing volcanic rift zones - the Koa'e fault system, Hawai'i, and the Krafla fissure swarm, NE Iceland - to compare and contrast evolving segmentation patterns during rift development. Field mapping reveals that surface-breaking faults in separate rift systems can follow different growth pathways during propagation. Faults that are located within *individual*

rift systems can also demonstrate differing growth patterns. Our new observations build on previous observations (e.g. Grant and Kattenhorn, 2004; Holland et al., 2006; Martel and Langley, 2006; Kaven and Martel, 2007), and extend models, conceptually, for fault growth in layered basaltic sequences.

## **2.1. Background: near-surface faults in layered basaltic sequences**

Existing studies of near-surface normal fault development in layered basaltic sequences identify four principal characteristics: (1) sinuous zones of vertical extension fractures (dominantly in the footwall, but also in the hanging wall); (2) monoclinical folding of the ground surface; (3) sub-vertical, surface-breaking fault scarps that show a component of dilation; and (4) less commonly, hanging wall buckles found proximally to the scarp bases (Duffield, 1975; Acocella et al., 2000; Grant and Kattenhorn, 2004; Martel and Langley, 2006; Holland et al., 2006; Villemain and Bergerat, 2013). These characteristics are expected to show predictable geometries, resulting from the following successive stages: (1) nucleation of a normal fault at depth; (2) slip on the fault at depth drives both folding of the free surface into a monocline, and tensile stress concentrations that result in the opening of pre-existing cooling joints in the footwall ahead of the fault tip; (3) with continued slip and upward propagation, the monocline becomes steeper and narrower, and footwall fractures widen and propagate downwards; (4) eventual linkage of surface extension fractures with fault tips at depth leads to systematic breaching of surface monoclines and the development of sub-vertical, surface-breaking fault segments that display horizontal and vertical components of displacement. Previous work has also invoked a downward fault growth model to account for fault patterns in basaltic sequences (e.g. Opheim and Gudmundsson, 1989). Here, we focus on the upward propagation model, which is more strongly supported by existing field



93 observations and numerical models (e.g. Grant and Kattenhorn, 2004; Martel and Langley, 2006;  
94 Kaven and Martel, 2007).

95       Based on upward growth models, we might expect predicted geometries (i.e. monoclinial  
96 folding of basaltic layering) to be preserved at depth following upward propagation of blind normal  
97 faults (e.g. Holland et al., 2006). Notably, field studies of exhumed basaltic fault zones have found  
98 little evidence for folding, implying that they may not represent precursory features of all basalt-  
99 hosted normal faults (e.g. Walker et al., 2012, 2013).

100       To date, an upward growth model has been broadly applied to normal fault growth in  
101 cohesive sequences for a range of geological settings on Earth, including the Koa'e fault system,  
102 Hawai'i (e.g. Holland et al., 2006; Podolsky and Roberts, 2008), Iceland (e.g. Grant and  
103 Kattenhorn, 2004; Villemin and Bergerat, 2013), the East Africa Rift (e.g. Casey et al., 2006;  
104 Rowland et al., 2007), mid ocean ridges (e.g. Soule et al., 2009; Escartin et al., 2016), and on other  
105 planets, including: Mars (e.g. Caparelli et al., 2007; Tanaka et al., 2008; Schultz et al., 2010),  
106 Enceladus (e.g. Nahm and Kattenhorn, 2015) and Earth's Moon (e.g. Nahm and Schultz, 2015).  
107 Most of the models derived for these systems involve a deforming volume that is mechanically  
108 isotropic, and undergoes uniformly applied boundary stresses at a constant strain rate. Using  
109 detailed field observations of surface structures in the Koa'e fault system, Hawai'i and the Krafla  
110 fissure swarm in northern Iceland, we build upon the existing field-data-constrained numerical  
111 models of Martel and Langley (2006) and demonstrate that there is an inherently four-dimensional  
112 distribution of extensional strains and strain rates within developing volcanic rift zones. Our aim  
113 is to show that the evolving first-order geometry and distribution of normal faults is sensitive to  
114 variations in boundary stress conditions and the mechanical properties of the deforming sequence.

## 2.2. Methods

Surface structures in the Koa'e and Krafla fault systems were mapped using a combination of high resolution aerial images (GoogleEarth™ and World-View2: 0.5 m resolution), topographic datasets (aerial LiDAR: 0.5 m resolution (Koa'e only)), and traditional field mapping techniques. At the free surface, in both study areas, extension fractures (hereafter, *fractures*) appear to have initiated along pre-existing cooling joints in the lava pile, producing characteristic zigzag trace geometries (Figure 1). This is consistent with geometries that have previously been identified (e.g. Grant and Kattenhorn, 2004; Martel and Langley, 2006; Villemin and Bergerat, 2013).

*FIGURE 1 HERE*

This zig-zag geometry presents multiple piercing points in plan view, allowing displaced walls to be matched across the open fracture aperture (less than ~3 m; beyond this width, erosion and collapse can alter the fracture profile), and hence, accurate measurement of the following (see Figure 1): (1) extension direction and mode (extension, mode-I; extensional-shear, mixed-mode); (2) the amount of horizontal opening across the fracture, here referred to as fracture aperture; (3) fracture trace azimuth, equivalent to the strike of the fault plane; and (4) vertical offset of the free surface, where present. Remote and field data are combined to characterise the distribution, and geometry of fractures and surface-breaking normal faults, as well as monocline distribution, extent, and geometry to sub-metre precision and accuracy.

## 3. Surface-breaking fault systems in volcanic rift zones

### 3.1. Early stage rift development: The Koa'e fault system, Hawai'i

The Koa'e fault system borders the south flank of Kīlauea Volcano (Figure 2A), which is the youngest and southernmost subaerial volcano in the Hawaiian-Emperor chain, and one of five volcanic systems on the Island of Hawai'i (Neal and Lockwood, 2003). Melting, generated by an upwelling mantle plume, impinges on the lithosphere, through which magma ascends via a system of conduits into a series of interconnected shallow storage reservoirs at ~2.5-4 km and at ~2 km depth beneath Kīlauea's summit (e.g. Baker and Amelung, 2012; Lin et al., 2014). Repeated influx of magma into these storage reservoirs, at rates of  $\sim 0.1 \text{ km}^3 \text{ y}^{-1}$  (Swanson et al., 1976; Dzurisin et al., 1984; Poland et al., 2014), typically results in episodes of inflation and deflation, driving eruptive episodes either at the summit, or shallow intrusion and eruption within two pronounced rift zones: the Southwest and East Rift Zones (Figure 2A,B), which radiate south-westward and eastward from the summit (Duffield et al., 1982; Wright and Klein, 2006; Poland et al., 2012). Records of sustained eruptions at Kīlauea's summit show that the duration and volume of magma associated with eruptive episodes can vary significantly: In June 1952,  $38 \times 10^6 \text{ m}^3$  of magma was erupted over 136 days and in November 1967,  $64 \times 10^6 \text{ m}^3$  of magma was erupted over 251 days. Between 1983-2003, Kīlauea was in a phase of continuous eruption with  $\sim 200 \times 10^6 \text{ m}^3$  of magma released (Dvorak and Dzurisin, 1993; Poland et al., 2012). As a result of complex dynamics of the system, extension rates across Kīlauea also vary considerably from:  $\sim 26 \text{ cm/y}^{-1}$  between 1975-1983 to  $<5 \text{ cm/y}^{-1}$  since 1983 (Delaney et al., 1990, 1998). Flank displacement is linked to periods of shallow intrusion within the rift zones and summit region, and/or periods of gravitational sliding on a basal detachment at a depth of approximately 9 km (e.g. Klein et al., 1987; Delaney et al., 1990; Denlinger and Okubo, 1995; Le Corvec and Walter, 2009).

*FIGURE 2 HERE*

Our study area is within the Koa'e fault system, which is a 12 km long, ~3 km wide zone of normal faulting (Figure 2A), that connects the Southwest and East Rift Zones (SWRZ and ERZ, hereafter) to form a continuous, 60-70 km long, ENE-WSW trending zone of extension. Normal faults in the system are growth faults, interpreted to be related both to the forceful emplacement of dykes into the rift zones of Kīlauea Volcano (Duffield et al., 1975, 1982; Swanson et al 1976; Peacock and Parfitt, 2002) and to gravitationally induced volcano spreading (Poland et al., 2014 and references therein). The area is characterized by small-volume tholeiitic pahoehoe type lavas, emplaced as inflated sheets, onto the subhorizontal (1-2°) volcano flank. Individual lava thickness is highly variable. Cross-sectional views, normal to the lava flow direction, show maximum thicknesses of up to 4 m (e.g., Hon et al., 1994; Bubeck et al., 2017a), but taper laterally to tens-of-centimetre thicknesses at the tens-of-metre to hundred-metre length scales.

### **3.1.1. Surface structures in the Koa'e fault system**

Mapping in the Koa'e fault system reveals three characteristic structures (Figure 2B): (1) ENE-WSW striking (ERZ-parallel) faults, with sub-vertical NNW-dipping scarps that show maximum throws of 12-16 m; (2) fracture networks that are grouped into two orientations: ENE-WSW (ERZ-parallel) and NW-SE (ERZ-oblique); and (3) N to NNW-dipping monoclinial folds, which are discontinuous, show variable amplitudes of up to 12 m, and have crests that are parallel to the strike of major normal faults and the strike of the ERZ. ENE-WSW striking fractures dominate in the Koa'e whereas NW-SE striking fracture sets form obliquely oriented steps along fracture (cm-10s of m scale) and fault (hundreds of metre, to km scale) traces (Bubeck et al., 2017b). An additional feature located in the immediate hanging wall of some faults are localized buckle

structures with anticlinal crests that parallel the strike of the ERZ and show amplitudes of up to 2 m.

Fracture networks form sinuous zones up to ~5 km in length and 30-50 m wide (Figure 3A). Most of these zones are limited to the footwalls of surface-breaking normal faults and along the upper limb of monoclines, where they parallel the strike of the fold crest. Less commonly, fractures are found in the hanging walls of faults, and as isolated zones in areas of the fault system where fault scarps are absent and there is no evidence for monoclinal flexure of the surface (Figure 3B, C; Figure 4A).

#### *FIGURE 3 HERE*

A summary of orientation and kinematic data for fractures and normal faults are presented here; more detailed orientation, aperture and kinematic data are presented in Bubeck et al. (2017b).

Zones of rift-parallel (ENE-WSW) fractures are most common (~85% of mapped traces) and show individual fracture trace lengths of up to ~370 m. Apertures may be as much as ~4 m, but are more commonly in the range of 0.3-0.6 m (Bubeck et al., 2017b). NW-SE striking fracture zones are less common (~15% of mapped traces) with individual fracture trace lengths of ~4-120 m and apertures of 0.02-2.50 m (Bubeck et al., 2017b). Field characterization of fractures in the study identified only extensional openings (i.e. orthogonal to fracture azimuth; e.g. Figure 1) and we recorded no preferred stepping direction between segmented fracture traces. NW-SE striking fractures tend to occur in close association with the lateral terminations of rift-parallel normal faults and footwall fractures, occurring as obliquely oriented steps or linkages between segments (Figure 2B; Bubeck et al., 2017b). Individual fractures that outcrop for >10 m (e.g. Figure 3A, B; Figure 4) in the study area commonly display multiple steps along their length in plan view,

suggesting they represent composite fractures produced by linkage of segments (e.g. Peacock and Sanderson, 1991). At the scale of the individual fractures (i.e. beyond the scale of joint-related irregularities), shorter fractures (<10 m in length) also display non-linear traces with obliquely oriented steps, hook-shaped tips, or abutting geometries in the vicinity of neighboring structures (Figure 3C). Fractures of this length scale are most commonly found along the upper limbs of monoclines where they form distributed networks (Figure 3A, 4B). In some instances, these networks are set back from the region of present day maximum curvature (Figure 4B) and elsewhere they follow regions of maximum curvature on monocline limbs (Figure 4C).

*FIGURE 4 HERE*

Monoclinial folds in the Koa'e fault system may be divided into two scales: (1) monoclines that are laterally continuous at the kilometre scale, for distances up to 3 km (Figure 2B, 5A); and (2) monoclines that are laterally discontinuous, with maximum lengths of ~150 m (Figure 2B, 5B). Continuous monoclines are observed in the western and central-western areas of the fault system (Figure 2B); folds show rounded morphologies with amplitudes of up to ~16 m (Figure 5A, 6A-C) and limbs dip gently (typically ~15° but, locally up to ~25 °) (Figure 6D, 7A).

*FIGURE 5 HERE*

This is in agreement with the models of Martel and Langley (2006) and Kaven and Martel (2007) who predicted monoclines will steepen as faults approach the free surface. Such patterns were also recorded by Podolsky and Roberts (2008) along the White Rabbit Fault (Figure 2b); these authors,

however, instead linked along-strike variations in monocline amplitude to local occurrence of relay ramps ahead of the tips of previously soft-linked segments, rather than to upward propagation-related folding.

*FIGURE 6 HERE*

Such fault tip monoclines are particularly clear along the Ohale Pali (Figure 2B) where discontinuous folds occur as isolated lenses caught between en echelon fault segments (Figure 7B). The monoclines described in this study, however, are distinct from this relay ramp tilting mechanism.

Discontinuous monoclines are restricted to the eastern region of the Koa'e fault system, and are most common along the Kulanaokuaiki Fault (Figure 2B) where they form isolated, often disintegrated blocks with maximum amplitudes of up to ~15 m in the centre of each block, decreasing steeply (~30°) to zero at the lateral tips (Figure 5B, 7C). Breached examples were not observed. The hanging wall free surface that is offset across adjacent fault scarps is relatively planar. The width of the folded limb of these structures does not vary greatly, ranging from 10 to 20 m. These monoclines feature large (often >4 m wide) composite fractures along their upper limb and tend to be connected laterally with large, open fault scarps with vertical offsets up to 12 m. Monoclines of this type are decoupled from the footwall along these continuous co-linear composite extension fractures (Figure 5B, 7C). The limited lateral extent of the short monoclines, fragmented appearance, and localised steep dip are consistent with a fault-bound block rotation of the immediate hanging wall, effected by blind antithetic faults rather than a monoclinal fold. Such

rotational features have been produced in analogue models of fault propagation in brittle sequences (e.g. Holland et al., 2006; Michie et al., 2014).

*FIGURE 7 HERE*

Where present, neither type of monocline has been systematically breached, despite being parallel to the strike of prominent normal faults in the region (Figure 2B). Where breaching has been observed, vertical offsets on the monocline-breaching segments are minor (up to 6 m) (Figure 6B) compared to collinear fault scarps (up to 16 m throw) (Figure 8).

Where present, sub-vertical normal faults in the area typically offset the surface by up to ~15 m (Figure 5B, Figure 7). In addition to a vertical component of displacement, all surface-breaking fault segments exhibit horizontal openings along composite fracture traces with apertures of up to ~5 m. Fault scarps preserve cooling joint-related irregularities (e.g. Figure 1) and we find no evidence for slickenlines or slickensides on fracture surfaces to indicate initial shear displacement, consistent with observations in previous studies (e.g. Holland et al., 2006; Peacock and Parfitt, 2002).

*FIGURE 8 HERE*

It is not possible to determine from field study alone whether fault slip at depth was purely dip-slip. Seismicity records suggest that strike-slip and oblique-slip faulting is common at depths of 0.5-5.0 km below the Koa'e fault system (Lin and Okubo, 2016), but the surface expression of this on the mapped faults is unclear. Mapping has revealed that surface-breaking normal fault



segments (up to 200 m in length) are most commonly found in the central-eastern and eastern regions of the fault system, within ~5 km of the upper ERZ. Based on the total lengths of deformation zones (up to 5 km; Figure 2B), our interpretation of these segments is that they represent discontinuous splays of single fault structures at depth. Based on remote mapping techniques, surface-breaking fault segments that offset planar footwall and hanging wall surfaces are estimated to comprise approximately 20% of inferred fault traces in the Koa'e fault system; the remaining ~80% is characterised by monoclinal folding, blind normal faults, and rarely, monocline-breaching fault segments.

### **3.2. Advanced stage rift development: The Krafla fissure swarm, Iceland**

Iceland is located on the plate boundary between North America and Eurasia, and represents a subaerially exposed segment of the Mid-Atlantic Ridge. The Icelandic axial rift zone (the Neovolcanic Zone: NVZ) accommodates WNW-ESE (104°) extension of ~19 mm/year (e.g. Sæmundsson, 1974; Wright et al., 2012) across 5 sub-parallel NNE-SSW-striking en echelon volcanic systems and associated fissure swarms: Theistareykir, Krafla, Fremri-Namur, Askja, and Kverkfjöll (Figure 8A). Extension in these zones is accommodated by systems of normal faults, sub-parallel eruptive fissures, and extension fractures that radiate outward from axial volcanoes in a direction orthogonal to the regional minimum horizontal stress (e.g. Sæmundsson, 1974; Brandsdóttir and Einarsson, 1979). The Krafla central volcano and associated fault and fracture networks have dominated volcanic activity in the axial rift zone, with approximately 35 Holocene basaltic eruptions identified (Brandsdóttir and Einarsson, 1979; Opheim and Gudmundsson, 1989). The rift zone extends 80-100 km along strike (Figure 9A), with a width of 4-10 km (Bjornsson et al., 2007).

Magma is stored beneath the central volcano, in a reservoir at approximately 2.5-3.0 km depth and supplied at a rate of  $\sim 1.6 \text{ km}^3$  per year (Tryggvason, 1986; Dauteuil et al., 2001). Records of ground deformation, dating back to 1976, highlight pronounced and repeated episodes of steady inflation followed by rapid deflation (and subsidence), associated with rift zone extension (Bjornsson et al., 1978; Tryggvason, 1984; Rubin, 1992). The scale and duration of these episodes is highly variable. For instance,  $30\text{-}40 \times 10^6 \text{ m}^3$  was erupted from Krafla in 1980 over a period of 12 hours. In another episode deflation of the summit reservoir released  $198 \times 10^6 \text{ m}^3$  over 39 days. During those events, large portions of the rift zone are known to have extended: between 1974-78, up to eight separate inflation-deflation events were recorded and 80-90 km of the  $\sim 100$  km long rift zone accommodated extension (Tryggvason, 1984). Lateral dyke propagation has been recorded for large distances ( $\sim 50$  km) along the rift zone (Bjornsson et al., 1978; Buck et al., 2006; Hjartardóttir et al., 2012). Based on the ages for lava flows and erosional surfaces, deformation rates are estimated to be between  $1.5\text{-}15 \text{ cm/y}^{-1}$  (Dauteuil et al., 2001). Lavas in the study area dominantly are of pahoehoe type, with individual unit thickness ranging from  $\sim 10$  cm, up to  $\sim 3$  m. Lava thicknesses in the study area are reasonably constant ( $\pm 10\%$ ) over the hundred-metre length scale.

*FIGURE 9 HERE*

### **3.2.1. Surface structures in the Krafla fissure swarm**

Here we focus on an area of the Krafla rift system  $\sim 10$  km north of Krafla Volcano (Figure 9B, C). Detailed measurements of orientation, kinematics and aperture of fractures and normal faults are presented in Bubeck et al. (2017b); here we provide a summary. Mapping reveals the following

structures (Figure 9C, D): (1) rift zone-parallel (NNE-SSW strike) normal faults, with sub-vertical scarps that dip to the WNW and ESE, and accommodate displacements >15 m; (2) networks of fractures found dominantly within the footwall (and less commonly in the hanging wall) of surface-breaking normal faults; and (3) rarely, monoclinical folds and hanging wall buckles. Fractures are grouped into three dominant strike orientations (Figure 9D): NNE-SSW (rift-parallel), NW-SE (rift-oblique), and WNW-ESE (rift-normal). Importantly, fractures with orientations outside of the principal rift trend (NNE-SSW) are not randomly distributed but show a close spatial association with the tips of en echelon rift faults (Bubeck et al. 2017b).

Fractures in the Krafla fissure swarm form linear zones that are up to 5 km long and 5-15 m wide. Rift-parallel striking fractures of this order are most common in the study area (~60% of mapped fracture traces) and show lengths of up to ~800 m, with apertures of up to 4 m, but commonly in the range 1.0-1.5 m (Bubeck et al., 2017b). Rift-oblique (NW-SE) striking fractures are less frequent (~30% of mapped fracture traces), but accommodate similar scales of opening (up to 4 m; modal opening is 2.0-2.5 m) across open fault scarps, with lengths up to ~50 m (Bubeck et al., 2017b). Rift-normal (WNW-ESE) striking fractures are least common (~10% of mapped fracture traces) and show the smallest lengths (less than ~40 m) and apertures (up to ~1 m) (Bubeck et al., 2017b). None of the fracture sets identified show a preferred stepping direction, and individual fractures show prominent obliquely-oriented steps in their traces, which commonly coincide with points of aperture minima. Such patterns have been interpreted previously elsewhere to represent sites of segment linkage between originally segmented structures (e.g. Peacock and Sanderson, 1991). At the scale of whole fractures (tens to hundreds of metre scale), traces are linear and considered composite structures: i.e. they represent coalesced fractures that were originally segmented.

345  
346 *FIGURE 10 HERE*  
347

348       Extension in the Krafla fissure swarm is accommodated dominantly by large (>15 m  
349 displacement), sub-vertical surface-breaking faults that offset planar footwall-hanging wall surfaces  
350 (Figure 10). Faults are continuous in length for 0.5-1.5 km and parallel to the NNE-SSW trend of  
351 the rift zone, accommodating WNW-ESE extension (Figure 9B, D). As observed in the Koa'e fault  
352 system, faults show significant horizontal openings of up to 4 m, in addition to a vertical component  
353 of displacement (Figure 9). A sub-set of shorter normal faults (<0.5 km length) and fractures, which  
354 strike at a low angle to the main rift trend (i.e. NW-SE), occurs at the terminations of rift-parallel  
355 faults (e.g. Figure 9B) (Bubeck et al., 2017b). Fractures in this trend show prominent strike-slip  
356 displacements, in addition to open components (Bubeck et al., 2017b). Strike-slip motion has not  
357 been observed across NW-SE striking fault segments, however it should be noted that the lack of  
358 preserved piercing points precludes documentation of any horizontal component of motion in this  
359 case.

360       Crests of monoclines are parallel to the NNE-SSW trend of the rift zone and strike of  
361 normal faults (Figure 9C, 11). Based on their spatial extent, only laterally discontinuous (<50 in  
362 length) monoclines are identified. Monoclines in the Krafla fissure swarm typically have low  
363 amplitudes (<10 m) and rounded morphologies, with open fractures along the upper limb, which  
364 are collinear with adjacent open normal fault scarps on either side of the monocline (Figure 11A).  
365 Breached monoclines are more common in the Krafla study area.

366  
367 *FIGURE 11 HERE*

Where monoclines are breached, amplitudes are generally low ( $<2$  m) and extensional strains have localised on the breaching fault segment, which in some instances, have accrued throws of 0.5-1.0 m (e.g. Figure 11B). Along one fault segment there is also evidence for multiple monocline geometries with the development of an additional fold further into the hanging wall, ahead of a breached monocline (Figure 11B). Instances of heavily fractured or disintegrated morphologies, though less common in the Krafla study area, show steep rotations of up to  $90^\circ$  (Figure 11C). Importantly, monoclines in the Krafla fissure swarm are comparatively rare and are associated with smaller rift-parallel striking faults (throw  $<15$  m), rather than representing characteristic features of all faults.

## **4. Discussion**

### **4.1. Comparison of surface structures in the Koa'e and Krafla fault systems**

Field observations of the distribution and geometry of normal faults in the Koa'e fault system and the Krafla fissure swarm show similar structural features to one another, and to existing predicted geometries (e.g. Grant and Kattenhorn, 2004; Holland et al., 2006; Martel and Langley, 2006; Kaven and Martel, 2007), including: (1) sub-vertical fault scarps with prominent openings (2-4 m); (2) monoclines that strike parallel to rift faults and decrease in width as they increase in height prior to breaching; and (3) zones of sub-vertical fractures that appear to activate pre-existing cooling joints. These shared structural features are predicted to follow a stepwise and systematic evolution with earlier features evident in advanced stages (e.g. Martel and Langley, 2006; Kaven and Martel, 2007).

In general, surface-breaking faults in the Krafla fissure swarm are larger (>15 m throw), longer (>500 m) and more prevalent than surface-breaking faults in the Koa'e. Extension fracture networks in the Koa'e are more distributed and comprise a greater number of shorter (between 10-20 m) and narrower (typically 0.3-0.6 m aperture) fractures. These characteristics lead us to consider that faults in the Krafla fissure swarm are in a more advanced stage of development, and accommodate greater strains than structures in the Koa'e fault system. We might therefore expect faults in both settings to follow the same evolutionary path, as has been suggested previously (e.g., Martel and Langley, 2006), with faults in Krafla to be in a more advanced stage of the same development process.

Our field observations, however, highlight prominent departures from both the predicted geometries in the models, and between the two locations; specifically, precursory monoclines are not present along all fault traces, where they ought to be systematically breached. In the Koa'e fault system, monoclines are not uniformly distributed, but rather they are restricted to central-western and western regions of the fault system (Figure 2B), where they form continuous structural features for up to ~3 km; amplitudes are similar to the surface-breaking fault segments in the eastern portions of the fault system. In the east of the fault system, within ~5 km of the upper ERZ, large (5-15 m throw) surface-breaking faults dominate and outcrop as subvertical scarps with open fractures at their base, with few instances of folding of the ground surface prior to breaching. The result of this distribution of deformation in the Koa'e is a pronounced east-west structure gradient. In the Krafla fissure swarm, monoclines are comparatively rare and associated with smaller displacement faults. They do not demonstrate a preferred spatial distribution. Surface-breaking normal faults on the other hand, are found up to 20 km away from the central volcano.

## 4.2. Controls on the surface expression of extensional structures

### 4.2.1. Syntectonic volcanism

Most numerical and scaled-analogue models of fault growth in cohesive sequences involve uniform, constant-rate displacement boundary conditions (e.g. Grant and Kattenhorn, 2004; Holland et al., 2006, 2011; Martel and Langley, 2006). Driving stresses, and hence, strain rates in both the Koa'e and Krafla rift settings, however, are neither uniformly distributed, nor constant through time. Extension in both areas is associated with repeated dyke injection events, the scale and timing of which are variable in time, space, and magnitude (e.g. Tryggvason, 1984; Dvorak and Dzurisin, 1993; Bjornsson et al., 2007; Delaney et al., 1998; Buck et al., 2006). Variable rates and duration of magma emplacement within the rift zones has the effect of altering local stress distributions, which in turn drives variations in strain rate and results in local strain rate gradients. This should be expected to influence segmentation patterns and fault architecture. The distribution of surface deformation styles in the Koa'e fault system may be a record of this.

*FIGURE 12 HERE*

Periods of inflation and deflation within Kīlauea's south flank have been linked with regions of elevated concomitant seismicity below the summit and upper ERZ (Figure 12) at ~2-5 km depth (e.g. Delaney et al., 1998; Hansen et al., 2004; Baker and Amelung, 2012; Lin and Okubo, 2016). Earthquake swarms originating in the upper ERZ have been recorded to migrate into the Koa'e fault system during intrusion events (Delaney et al., 1998), and in some instances linked to episodes of slip on major faults in the areas. The proximal distribution of surface-breaking faults in the eastern Koa'e fault system are therefore likely to be linked to these areas of elevated

436 seismicity and magma emplacement. For instance, records of GPS data, InSAR, and field  
437 observations, have revealed evidence for minor slip on the Kulanaokuaiki Fault during the  
438 September 1999 dyke intrusion event (Cervelli et al., 2002) (Figure 12). This is consistent with  
439 elastic dislocation models of the south flank that predict regions of high tensile stress  
440 concentrations that centre on the intruded region and extend into the eastern Koa'e (Owen et al  
441 2000; Cervelli et al., 2002). The scale and distribution of such stress concentrations become a  
442 function of the magnitude and location of the emplacement event, and hence, the resulting strain  
443 rate along the rift zone will vary accordingly. Magmatic and seismic activity in Kīlauea's SWRZ,  
444 by comparison, is significantly less (e.g. Dvorak and Dzurisin, 1993; Wauthier et al., 2016). During  
445 the period 2005-2007 inflation episode, for example, seismicity records indicate up to ~10 events  
446 per day in the SWRZ, compared to ~30 per day in the ERZ (Wauthier et al., 2016). Models of  
447 magma partitioning suggest that during the period 1840-1989, ~57% of magma supplied to the  
448 volcano was emplaced and erupted within the ERZ ( $1575 \times 10^6 \text{ m}^3$ ) with only ~2% ( $45 \times 10^6 \text{ m}^3$ )  
449 being erupted in the SWRZ (Dzurisin et al., 1984; Dvorak and Dzurisin, 1993). The result of this  
450 partitioning has led to more than 20 eruptions in the ERZ since 1950, associated with deflation of  
451 Kīlauea's summit reservoir, and only two events taking place in the SWRZ. Partitioning of  
452 extensional strain across the Koa'e fault system implies that total strains are comparable across the  
453 system, but spatially variable strain rates control whether faults are able to propagate straight to  
454 the surface (eastern Koa'e), or remain segmented at depth for protracted periods with slip  
455 accommodated aseismically, generating surface monoclines (western Koa'e). This is consistent  
456 with volcano-tectonic seismicity modelling from Kīlauea (e.g. Wauthier et al., 2016), and other  
457 volcanic faults (Toda et al., 2002; Roman and Gardine, 2013), which suggest that low rates of  
458 magma emplacement produce correspondingly low strain rates that are unable to drive significant



seismicity. With renewed magmatic partitioning into the SWRZ during future episodes, faults in western portions of the Koa‘e may therefore breach the surface and monoclines will be preserved in their hanging walls.

In contrast, the relatively minor abundance of monoclines and dominance of larger (>10 m throw) surface-breaking faults in the Krafla fissure swarm, up to 20 km away from the summit does not imply the presence of a spatial strain rate gradient, indicating magma supply here and related stresses are relatively uniform. Following re-surfacing, therefore, stresses and strain rates are high enough for fault segments to propagate straight to the surface without folding it first. The occurrence, however, of breached monoclines, though uncommon, suggests a temporal strain rate gradient can also exist. In evolving volcanic rift systems, therefore, the final geometry of first-order faults becomes a strain rate-dependent function of the magmatic processes taking place. This dependence becomes both a spatial problem as well as a temporal one.

#### **4.2.2. Mechanical stratigraphy**

In addition to magmatically induced segmentation patterns, host rock mechanical properties are also likely to play a role in the distribution and geometry of faults in the study areas. A prominent cooling joint fabric and mechanical layers, in the form of bedding and physical property variations (e.g. Planke, 1994; Bubeck et al., 2017a), mean that basaltic sequences are highly anisotropic and host a similarly pronounced mechanical stratigraphy as have been reported for layered clastic (e.g. Ferrill et al., 2017) and crystalline-clastic sequences (Walker et al., 2013). Existing studies of extensional fault geometry in mechanically layered sequences have shown that the mechanical properties of a deforming volume will govern segmentation patterns, and hence, the final architecture of fault zones (e.g. Peacock and Sanderson, 1991; Ferrill and Morris, 2003; Schöpfer

et al., 2006; Van Gent et al., 2010; Walker et al., 2013). At the metre-scale, anisotropy within basaltic sequences pertains to varying physical and mechanical properties within individual lava units or volcanoclastic horizons, as well as networks of pre-existing cooling joints. At the tens to hundreds of metre-scale, changes in compositional layering and fluid content within the sequence should also be expected to influence the distribution and geometry of surface structures in developing volcanic rift systems.

#### **4.3.A modified conceptual model for near-surface fault growth in basaltic sequences**

Here, we present conceptual models for near-surface fault growth, based on the natural distribution and geometry of extensional structures in the Koa'e and Krafla fault systems, as an expansion of the numerical models presented by Martel and Langley (2006) and Kaven and Martel (2007). As this model is based on surface observations only, stage I is based on theoretical models of dyke-fault relationships from volcanic settings. Depending on the distribution, magnitude, and duration of individual rifting episodes, fault zones may show variable overall geometries and associated fracture densities, as a function of spatial and temporal strain rate evolution. For this reason, stage III of this model is divided into two paths that are referred to here as: a high strain rate path and a low strain rate path.

*FIGURE 13 HERE*

**Stage I:** Initial extension may result from magma release during deflation of the central reservoir where high magma pressure will drive dykes into existing adjacent joints or discontinuities. At intermediate depths, upward (or lateral) propagation, governed by the hydrofracture criterion (e.g.

Gudmundsson, 2011), is impeded by the presence of mechanical barriers (e.g. Bell and Kilburn, 2012) or when driving pressures drop (e.g. Buck et al., 2006; Rowland et al., 2007). Dyke tip stresses are relieved by the growth of normal faults, which propagate along maximum tensile strain trajectories within the overlying basalt cover (e.g. Hollingsworth et al., 2013).

**Stage II:** In the region ahead of upward-propagating normal faults, at a critical distance from the free surface (controlled by the magnitude of the stress intensity at the fault tip), extension fractures begin to localise in linear zones along pre-existing cooling joints that are optimally oriented. These zones are parallel to the structures at depth and progressively lengthen downwards and laterally (Figure 13, Stage 1).

**Stage III (low strain rate):** During periods, or in regions of subdued magmatism, local driving stresses are too low to drive significant fault slip. Under these conditions, through-going linkage of fault tiplines at depth, and surface fractures, is prevented and faults will remain segmented at depth. Here, they will creep aseismically, producing monoclinal folding of the layers ahead of the tipline (Figure 13, Stage 2). With renewed magmatic activity, strain rates will increase once more and through-going linkage will be possible. During slip accumulation, and further upward propagation, surface monoclines will steepen until they are breached along newly linked fault-fracture networks (Figure 13, Stage 3).

**Stage III (high strain rate):** During periods, or in regions of elevated magmatism, or in the absence of resistant layers, linkage of upward propagating faults, and downward propagating fractures will result in through-going, surface-breaking faults. At this stage, extension is localised on a smaller number of larger structures, which dominate over new fracture growth: an exponential scaling is predicted (e.g. Ackerman et al., 2001). This process could take place relatively quickly

and result in through-going faults without folding of the surface (Figure 13, Stage 4). Seismicity data and eyewitness accounts, for instance, of the Kulanaokuaiki fault during the 1965 eruption of Kilauea Volcano, record evidence of crack propagation and vertical displacement occurring over the course of hours to days following the initial eruption (Fiske and Koyanagi, 1968).

In this model, monoclines are not necessarily precursory features of normal fault growth but rather a record of segmented growth, which may develop at any time within the series, depending largely on local strain rates. Breached monoclines, on the other hand, may imply a period, or region, of lower strain rate and segmentation followed by a sudden rate increase once more and through-going fault development.

An upward propagating fault model (e.g., Martel and Langley, 2006) is strongly supported by our field observations. Extension fractures are not randomly distributed across either fault system. In both settings, fractures are parallel to the trend of the rift zone and major rift faults and folds within it. Although fractures show a spatial relationship with fold curvature in some places, outer arc stretching is not the primary driving mechanism for their formation. A coupled evolution of fractures at the free surface and faults at depth, driven by stresses ahead of a blind fault tip is consistent with existing numerical predictions (e.g. Martel and Langley, 2006).

The growth of fault populations through time in developing volcanic rift systems, however, do not follow a uniform, systematic evolution; the distribution and geometry of normal faults in the Krafla fissure swarm are not always directly evolved equivalents of faults in the Koa'e fault system. This model may account for the apparent lack of preserved monoclines in exhumed basalt-hosted fault systems (e.g. Walker et al., 2012, 2013). Although factors including pre-existing structures and mechanical stratigraphy will influence the nucleation and initial geometry of fault

structures, changes in strain rate at any stage will alter the geometry and distribution of preserved faults.

## **5. Conclusions**

Current models for surface-breaking in faults in volcanic sequences dominantly invoke geometric or kinematic linkage as a progressive fault zone evolution. Our findings support existing models in a simple way: surface deformation is localized by normal faults that nucleate at depth and drive tensile stress concentrations ahead of the fault tip. Coupled upward propagation of fault tips at depth, and downward growth of surface fractures produces surface-breaking normal faults with prominent horizontal openings at their base. Contrary to model predictions, however, precursory monoclines are not systematic features of growth faults in basaltic sequences. We suggest that such deviations from model-predicted structural style and distribution can be explained by local variations in strain rate through time, and spatially within the actively deforming region. Strain rates within volcanic rift systems are genetically linked to magmatism and as such, surface-breaking faults within individual, or separate rift systems, may not experience a consistent evolution. Small displacement faults, therefore, will not necessarily be representative of the early stages of more evolved systems.

## **ACKNOWLEDGMENTS**

The authors wish to extend enormous gratitude to Don Swanson at the Hawaiian Volcano Observatory, Hawai'i, and Mike Poland (now at Cascades Volcano Observatory, Vancouver) for help and advice during field seasons to the Koa'e fault system. We further thank Don for taking the time to provide feedback on this manuscript and for generously sharing data with us. Authors Bubeck and Walker especially wish to thank Don for an unforgettable first tour of the Koa'e fault

system. We also thank the National Park Service for granting a permit to conduct fieldwork in the Koa`e fault system. Aerial LiDAR datasets were provided by the OpenTopography Facility with support from the National Science Foundation under NSF Award Numbers 1226353 & 1225810 (not related to this study). This research did not receive any specific grant from funding agencies in the public, commercial, or not-for-profit sectors. We thank Jonathan Bull for his review and extend special thanks to Michael Kettermann for his detailed and constructive review of an earlier version of this manuscript.

## FIGURES

**Figure 1.** Measurement of fracture geometry and kinematics: extension-mode opening across pre-existing cooling joint surfaces allows the traditional measurement of opening direction, aperture, azimuth and vertical offset (where present).

**Figure 2.** A. Simplified structural elements map of Kīlauea Volcano: Koa`e fault system (KFS); ERZ: East Rift Zone; SWRZ: Southwest Rift Zone; HFS: Hilina Fault System. Inset shows relative position of A, on the south coast of Hawai`i. B. Map of extensional structures in the Koa`e fault system: (1) surface-breaking normal faults (yellow lines); (2) extension fracture networks (orange lines); and (3) monoclinial folds with lengths >150 m (blue lines). Bi. Rose diagram highlights the strike direction of monoclines in the Koa`e fault system. Bii. Rose diagram highlights the strike direction of 1888 mapped fracture and faults in the Koa`e fault system. C. Lower hemisphere stereographic projections showing the average strike of fault/fractures and calculated maximum horizontal extension directions for the two dominant

orientations: i) ENE-WSW striking (ERZ-parallel) structures, accommodating NNW-SSE extension; ii) NW-SE striking (ERZ-oblique) structures accommodating NE-SW extension.

**Figure 3.** Scaling and location of extension fracture networks. A. At the 100's of metre-scale, fracture zones are predominantly located in the footwall of faults and along the upper limb of monoclines. Zones range from 30-50 in width and extend for >1 km. Base image: aerial World-View 2 satellite image (0.5 m resolution). Inset map indicates image locations for parts A, B and C. B. At the 10's of metre-scale fractures show stepped geometries and apertures of up to ~4 m. C. At the cm-scale, fractures also demonstrate stepping trace geometries and “hook-shaped” tip geometries in the vicinity of neighbouring fracture tips. At these scales, fractures are also observed in otherwise undeformed (i.e. not folded, non-faulted) regions of the fault system.

**Figure 4.** Maps of 3D surface curvature derived from aerial LiDAR datasets and examples of extension fracture distribution in the Koa'e fault system. A positive curvature (warm colours) indicates the surface is upwardly convex; a negative curvature (cold colours) indicates the surface is upwardly concave. A. Fracture networks are present in areas of the fault system where there is no topographic expression of fault slip (i.e. monoclines, or fault scarps). Anomalous regions of curvature are associated with tumuli and the general morphology of the lava field. B. Fracture networks occur along the upper limb of monoclines where they are not spatially associated with regions of maximum curvature across monoclines. C. Fracture networks show a strong spatial relationship with regions of maximum curvature across monoclines.

**Figure 5.** Examples of monocline type in the Koa'e fault system. Inset map indicates image locations for parts A and B. A. Laterally continuous monoclines with fold limbs that dip gently and vary from a 2 m to ~ 10 m in amplitude. Zones of fractures are found along the upper limbs and rubbly toes at the base. Crests can be traced for over 1 km. B. Laterally discontinuous monoclines form densely fractured, often disintegrated blocks in the hanging wall of faults. Lengths vary from 10 m to 150 m and amplitudes from 2 m to 15 m. Solid red line in part A highlights monocline profile. Dashed blue lines: extent of continuous monocline; dashed orange line indicates extent of discontinuous monocline; dashed red lines: continuous open fracture; dashed yellow lines: extent of hanging wall buckles.

**Figure 6.** A. Map view of the continuous monocline shown in Figure 5, showing the distribution of extension fractures along the upper limb (dotted red lines). For location, please refer to the inset map for Figure 5. B. Cross-sections across the monocline in part A. Transect locations are shown in part A. Transects 1-3 and 6 show steep, rounded monoclines with extension fractures along the region of maximum curvature. Transects 4 and 5 show a region of the monocline that has been breached by fault segments. The extent of this breaching is spatially limited. C: A map highlighting changes in 3D surface curvature across the monocline in part A. D. A slope map across the monocline in part A. Slope angles for the monocline limb range from ~12-25° with these values varying along-strike. Base image in A is an aerial World-View 2 satellite image (0.5 m resolution). Terrain data in parts C and D are derived from aerial LiDAR dataset (0.5 m resolution) provided by OpenTopography and generated in ArcGIS® software by Esri.



**Figure 7.** Map view of monocline types. A. Continuous monocline with a network of extension fractures along the upper limb. Limbs dip towards the north at  $\sim 10^\circ$ . Breached continuous monoclines are observed, but less commonly than unbreached. B. Fault tip monoclines between en echelon segments along the Ohale Fault. Tip monoclines dip parallel to the bounding segments by  $\sim 10^\circ$ . C. Discontinuous monocline blocks (dotted, yellow lines), isolated between normal fault segments (heavy red line), connected by collinear extension fractures (dotted red line) along the upper limb to form continuous open fractures that decouple the monocline from the footwall. These monoclines dip more steeply ( $\sim 30^\circ$ ) from a central amplitude maxima, to zero at the lateral edges. Breached discontinuous monoclines have not been observed. Base images: World-View 2 satellite image (0.5 m resolution).

**Figure 8.** Examples of surface-breaking normal fault segments in the Koa'e fault system. Inset map indicates location for images in Part A and B. A. The largest vertical offsets (up to  $\sim 15$  m) and greatest proportion of fault scarps are found on the Kulanaokuaiki ("Shaking Spine") fault. B. Where present, scarps show a significant component of horizontal opening and offset planar footwall and hanging wall ground surfaces. Also present along many (but not all) faults in the Koa'e fault system are hanging wall buckles that occur ahead of both fault scarps and monoclinal structures. Dashed orange line: extent of discontinuous monocline; dashed blue lines: extent of continuous monocline; dashed red lines: continuous open fracture; dashed yellow lines: extent of hanging wall buckles.

**Figure 9.** A. Map of Iceland highlighting the major tectonic elements: Reykjanes Ridge (RR); the Kolbeinsey Ridge (KR); West Volcanic Zone (WVZ); East Volcanic Zone (EVZ); Neo-

Volcanic Zone (NVZ: the axial rift zone); Askja volcanic centre (As); Fremri-Namur volcanic centre (Fr); Krafla volcanic centre, (highlighted blue; Kr); Theistareykir volcanic centre (Th); the Dalvik lineament (DF), the Husavik-Flatey Fault (HF) and the Grimsey lineament (GF). B. Location of study area in the Gjastykki Valley within the Krafla fissure swarm. C. Mapped faults and extension/oblique-extensional fractures in the study area. Image locations and view directions in Figures 10 and 11 are indicated. Ci. Rose diagram highlights the strike of normal faults and fractures in the Krafla fissure swarm. D. Lower hemisphere stereographic projections showing the average strike of fault/fractures and calculated maximum horizontal extension directions for the three dominant orientations: i) NNE-SSW striking faults and fractures, accommodating WNW-ESE extension; ii) WNW-ESE striking fractures, accommodating NNE-SSW extension; iii) NW-SE striking faults and fractures, accommodating ENE-WSW extension.

**Figure 10.** Examples of surface-breaking normal fault segments in the Gjastykki area of the Krafla fissure swarm. A. Subvertical normal faults with throws of up to 25-30 m and offset planar footwall and hanging wall surfaces. B. Rift faults show prominent horizontal openings of 2-4 m and overlapping geometries with obliquely-oriented linking segments.

**Figure 11.** Examples of monoclines in the Krafla fissure swarm. A. Monoclines show amplitudes of up to ~3 m with open fractures along their upper limbs that are co-linear with fault segments on either side. B. Breached monocline observed in the hangingwall of a surface-breaking normal fault with vertical offset of up 2-3 m. Along the fault in the image, an additional monocline has developed further into the hanging wall. C. Monoclines can also be strongly fragmented and show steep rotations. In all examples, their lateral extent is <50 m.

**Figure 12.** Distribution of surface-breaking normal faults and monoclinial folds across the Koa`e fault system. Blue circles represent focal mechanisms in the summit, upper ERZ, and upper SWRZ regions of Kīlauea Volcano from the period 1986-2009. Contours highlight the density of events based on approx. 3000 focal mechanisms recorded in this region. Earthquake data reproduced from Lin and Okubo, 2016. ~90% of focal mechanisms in the catalog are small earthquakes (96% <M2.5), from shallow depths (i.e. <13 km); half of the focal mechanisms are recorded from 2-5 km depth. Dyke intrusion events taken from Baker and Amelung, 2015 and Cervelli et al., 2002.

**Figure 13.** Conceptual model for growth faults in volcanic rift zones with spatially (and temporally) variable strain rates, with field examples of the model stages 1-4 from the Koa`e and Krafla fault systems. Principal stress axes (red arrows) represent the regional stress state acting on the rift zone. 1. Precursory extension fractures localize in narrow zones at the free surface ahead of blind normal faults. 2. In regions of the rift zone where strain rates are high, normal faults propagate rapidly upwards through the sequence and link with downward propagating surface fractures, producing fault scarps. A lack of preserved monocline indicates strain rates have remained high since the last resurfacing event. Antithetic faults may develop from points of stress concentration, causing a rotation of the hanging wall block above them. 3. In regions of the rift zone where strain rates are low, faults remain at depth where they accumulate slip aperiodically and gradually deform the free surface ahead of the tip line into monoclines. 4. In regions of the rift zone that experience episodically high strain rates, faults may spend protracted periods segmented at depth, followed by a rapid propagation phase that results in linkage with surface fractures and breaching of earlier formed monoclines at the free surface.

708

709 **REFERENCES CITED**

710 Ackermann, R. V., Schlische, R. W. & Withjack, M. O. 2001. The geometric and statistical

711 evolution of normal fault systems: an experimental study of the effects of mechanical layer

712 thickness on scaling laws. *Journal of Structural Geology*, 23, 1803-1819.

713 Acocella, V., Gudmundsson, A. & Funicello, R. 2000. Interaction and linkage of extension

714 fractures and normal faults: examples from the rift zone of Iceland. *Journal of Structural*

715 *Geology*, 22, 1233-1246.

716 Anderson, S. R. & Bowers, B. 1995. Stratigraphy of the unsaturated zone and uppermost part of

717 the Snake River Plain aquifer at Test Area North, Idaho National Engineering Laboratory,

718 Idaho. *Water Resources Investigations Report 95-4130*. US Geological Survey.

719 Baker, S. & Amelung, F. 2012. Top-down inflation and deflation at the summit of Kīlauea

720 Volcano, Hawai‘i observed with InSAR. *Journal of Geophysical Research: Solid Earth*, 117,

721 n/a-n/a.

722 Bell, A. F. & Kilburn, C. R. J. 2012. Precursors to dyke-fed eruptions at basaltic volcanoes:

723 insights from patterns of volcano-tectonic seismicity at Kilauea volcano, Hawaii. *Bulletin of*

724 *Volcanology*, 74, 325-339.

725 Bjornsson, A., Johnsen, G., Sigurdsson, S., Thorbergsson, G. & Tryggvason, E. 1978. Rifting of

726 the plate boundary in North Iceland 1975-1978. National Energy Authority Report 0S-JHD-78-

727 21. Nordic Volcanological Institute: University of Iceland.

728 Bjornsson, A., Saemundsson, K., Sigmundsson, F., Halldorsson, P., Sigbjornsson, R. &

729 Snaebjornsson, J. T. 2007. Geothermal projects in NE Iceland at Krafla, Bjarnarflag, Gjastykki

730 and Theistareykir: assessment of geo-hazards affecting energy production and transmission

731 systems emphasizing structural design criteria and mitigation of risk. Landsvirkjun report LV-  
732 2007/075.

733 Brandsdottir, B. & Einarsson, P. 1979. Seismic activity associated with the September 1977  
734 deflation of the Krafla central volcano in north-eastern Iceland. *Journal of Volcanology and*  
735 *Geothermal Research*, 6, 197-212.

736 Bubeck, A., Walker, R. J., Healy, D., Dobbs, M. & Holwell, D. A. 2017a. Pore geometry as a  
737 control on rock strength. *Earth and Planetary Science Letters*, 457, 38-48.

738 Bubeck, A., Walker, R. J., Imber, J., Holdsworth, R. E., MacLeod, C. J., & Holwell, D. A.  
739 2017b. Extension parallel to the rift zone during segmented fault growth: application to the  
740 evolution of the NE Atlantic. *Solid Earth*, 8(6), 1161.

741 Buck, W. R., Einarsson, P. & Brandsdóttir, B. 2006. Tectonic stress and magma chamber size as  
742 controls on dike propagation: Constraints from the 1975–1984 Krafla rifting episode. *Journal*  
743 *of Geophysical Research*, 111, 1-15.

744 Caprarello, G., Pondrelli, M., Di Lorenzo, S., Marinangeli, L., Ori, G. G., Greeley, R., & Neukum,  
745 G. (2007). A description of surface features in north Tyrrhena Terra, Mars: Evidence for  
746 extension and lava flooding. *Icarus*, 191(2), 524-544.

747 Casey, M., Ebinger, C., Keir, D., Gloaguen, R. & Mohamed, F. (eds.) 2006. *Strain*  
748 *accommodation in transitional rifts: extension by magma intrusion and faulting in Ethiopian*  
749 *rift magmatic segments*, The Geological Society of London: Geological Society, London,  
750 Special Publications.

751 Cervelli, P., Segall, P., Amelung, F., Garbeil, H., Meertens, C., Owen, S., Miklius, A. &  
752 Lisowski, M. 2002. The 12 September 1999 Upper East Rift Zone dike intrusion at Kilauea  
753 Volcano, Hawaii. *Journal of Geophysical Research: Solid Earth*, 107, ECV 3-1-ECV 3-13.

754 Crider, J. G. & Pollard, D. D. 1998. Fault linkage: Three-dimensional mechanical interaction  
755 between echelon normal faults. *Journal of Geophysical Research*, 103, 24,373-24,391.

756 Dauteuil, O., Angelier, J., Bergerat, F., Verrier, S. & Villemin, T. 2001. Deformation partitioning  
757 inside a fissure swarm of the northern icelandic rift. *Journal of Structural Geology*, 23, 1359-  
758 1372.

759 Davison, I., Stasiuk, S., Nuttall, P. & Keane, P. 2004. Sub-basalt hydrocarbon prospectivity in the  
760 Rockall, Faroe-Shetland and Møre Basins, NE Atlantic. Geological Society London. In: Vining,  
761 B.A. and Pickering, S.C. (eds.) *Petroleum Geology: from mature basins to new frontiers.*  
762 *Proceedings of the 7<sup>th</sup> Petroleum Geology Conference*, 1025-1032. Petroleum Geology  
763 Conferences Ltd, published by the Geological Society, London.

764 Delaney, P. T., Denlinger, R. P., Lisowski, M., Miklius, A., Okubo, P. G., Okamura, A. T. & Sako,  
765 M. K. 1998. Volcanic Spreading at Kilauea, 1976–1996. *Journal of Geophysical Research*, 103,  
766 18,003-18,023.

767 Delaney, P. T., Fiske, R. S., Miklius, A., Okamura, A. T. & Sako, M. K. 1990. Deep magma  
768 body beneath the summit and rift zones of Kilauea Volcano, Hawaii. *Science* 247.4948  
769 (1990): 1311-1316.

770 Denlinger, R. P. & Okubo, P. G. 1995. Structure of the mobile south flank of Kilauea Volcano,  
771 Hawaii. *Journal of Geophysical Research*, 100, 24499.

772 Duffield, W. A. 1975. Structure and Origin of the Koae Fault System, Kilauea Volcano, Hawaii.  
773 *Geological Survey Professional Paper* 856.

774 Duffield, W. A., Christiansen, R. L., Koyanagi, R. Y. & Peterson, D. W. 1982a. Storage, migration  
775 and eruption of magma at Kilauea Volcano, Hawaii, 1971-1972. *Journal of Volcanology and*  
776 *Geothermal Research*, 13, 273-307.

777 Dvorak, J. J. & Dzurisin, D. 1993. Variations in Magma Supply Rate at Kilauea Volcano, Hawaii.  
778 *Journal of Geophysical Research-Solid Earth*, 98, 22255-22268.

779 Dzurisin, D., Koyanagi, R. Y. & English, T. T. 1984. Magma supply and storage at Kilauea  
780 Volcano, Hawaii, 1956-1983. *Journal of Volcanology and Geothermal Research*, 21, 177-206.

781 Escartín, J., Leclerc, F., Olive, J. A., Mevel, C., Cannat, M., Petersen, S., Augustin, N., Feuillet,  
782 N., Deplus, C., Bezos, A., Bonnemaïn, D., Chavagnac, V., Choi, Y., Godard, M., Haaga, K.  
783 A., Hamelin, C., Ildefonse, B., Jamieson, J. W., John, B. E., Leleu, T., Macleod, C. J.,  
784 Massot-Campos, M., Nomikou, P., Paquet, M., Rommevaux-Jestin, C., Rothenbeck, M.,  
785 Steinführer, A., Tominaga, M., Triebe, L., Campos, R., Gracias, N., Garcia, R., Andreani, M.  
786 & Vilaseca, G. 2016. First direct observation of coseismic slip and seafloor rupture along a  
787 submarine normal fault and implications for fault slip history. *Earth and Planetary Science*  
788 *Letters*, 450, 96-107.

789 Faulds, J. E. & Varga, R. J. 1998. The role of accommodation zones and transfer zones in the  
790 regional segmentation of extended terranes. In: Faulds, J. E. and Stewart, J. H. (eds.)  
791 Accommodation Zones and Transfer Zones: the Regional Segmentation of the Basin and Range  
792 Province: Boulder, Colorado. *Geological Society of America Special Paper* 323, 1-45.

793 Ferrill, D. A. & Morris, A. P. 2001. Displacement gradient and deformation in normal fault  
794 systems. *Journal of Structural Geology*, 23, 619-638.

795 Ferrill, D. A. & Morris, A. P. 2003. Dilational normal faults. *Journal of Structural Geology*, 25,  
796 183-196.

797 Ferrill, D. A., Morris, A. P., McGinnis, R. N., Smart, K. J., Wigginton, S. S. & Hill, N. J. 2017.  
798 Mechanical stratigraphy and normal faulting. *Journal of Structural Geology*, 94, 275-302.

799 Fiske R.S., Koyanagi R.Y. 1968. The December 1965 Eruption of Kilauea Volcano, Hawaii.  
800 Geological Survey Professional Paper. No. 607, 1-21.

801 Forslund, T. & Gudmundsson, A. 1991. Crustal spreading due to dikes and faults in southwest  
802 Iceland. *Journal of Structural Geology*, 13, 443-457.

803 Grant, J. V. & Kattenhorn, S. A. 2004. Evolution of vertical faults at an extensional plate  
804 boundary, southwest Iceland. *Journal of Structural Geology*, 26, 537-557.

805 Gudmundsson, A. 2011. *Rock Fractures in Geological Processes*, Cambridge, UK, Cambridge  
806 University Press.

807 Hansen, S., Thurber, M., Mandernach, F., Haslinger, F. & Doran, C. 2004. Seismic velocity and  
808 attenuation structure of the East Rift Zone and south flank of Kilauea Volcano, Hawaii.  
809 *Bulletin of the seismological society of america*, 94.

810 Hauber, E., Grott, M., & Kronberg, P. (2010). Martian rifts: Structural geology and  
811 geophysics. *Earth and Planetary Science Letters*, 294(3-4), 393-410.

812 Helm-Clark, C. M., Rodgers, D. W. & Smith, R. P. 2004. Borehole geophysical techniques to  
813 define stratigraphy, alteration and aquifers in basalt. *Journal of Applied Geophysics*, 55, 3-38.

814 Hjartardóttir, Á. R., Einarsson, P., Bramham, E. & Wright, T. J. 2012. The Krafla fissure swarm,  
815 Iceland, and its formation by rifting events. *Bulletin of Volcanology*, 74, 2139-2153.

816 Holland, M., Urai, J. L. & Martel, S. J. 2006. The internal structure of fault zones in basaltic  
817 sequences. *Earth and Planetary Science Letters*, 248, 301-315.

818 Hollingsworth, J., Leprince, S., Ayoub, F. & Avouac, J. P. 2013. New constraints on dike  
819 injection and fault slip during the 1975-1984 Krafla rift crisis, NE Iceland. *Journal of*  
820 *Geophysical Research: Solid Earth*, 118, 3707-3727.



821 Hus, R., De Batist, M., Klerkx, J. & Matton, C. 2006. Fault linkage in continental rifts: structure  
822 and evolution of a large relay ramp in Zavarotny; Lake Baikal (Russia). *Journal of Structural*  
823 *Geology*, 28, 1338-1351.

824 Kaven, J. O. & Martel, S. J. 2007. Growth of surface-breaching normal faults as a three-  
825 dimensional fracturing process. *Journal of Structural Geology*, 29, 1463-1476.

826 Klein, F. W., Koyanagi, R. Y., Nakata, J. S. & Tanigawa, W. R. 1987. Volcanism in Hawaii. In:  
827 Decker, R. W., Wright, T. L. and Stuaffer, P. H. (eds.) US Geological Survey Professional  
828 Paper 1350.

829 Lambiase, J. J. & Bosworth, W. 1995. Structural controls on sedimentation in continental rifts.  
830 In: LAMBIASE, J. J. (ed.) Hydrocarbon habitat in rift basins. Geological Society Special  
831 Publication no. 80. The Geological Society, London.

832 Le Corvec, N. & Walter, T. R. 2009. Volcano spreading and fault interaction influenced by rift  
833 zone intrusions: Insights from analogue experiments analyzed with digital image correlation  
834 technique. *Journal of Volcanology and Geothermal Research*, 183, 170-182.

835 Lin, G. & Okubo, P. G. 2016. A large refined catalog of earthquake relocations and focal  
836 mechanisms for the Island of Hawai‘i and its seismotectonic implications. *Journal of*  
837 *Geophysical Research: Solid Earth*.

838 Lin, G., Amelung, F., Lavallee, Y. & Okubo, P. G. 2014. Seismic evidence for a crustal magma  
839 reservoir beneath the upper east rift zone of Kilauea volcano, Hawaii. *Geology*, 42, 187-190.

840 Long, J. J. & Imber, J. 2010. Geometrically coherent continuous deformation in the volume  
841 surrounding a seismically imaged normal fault-array. *Journal of Structural Geology*, 32, 222-  
842 234.

843 Maerten, L., Gillespie, P. & Pollard, D. D. 2002. Effects of local stress perturbation on secondary  
844 fault development. *Journal of Structural Geology*, 24, 145-153.

845 Manzocchi, T., Childs, C. & Walsh, J. J. 2010. Faults and fault properties in hydrocarbon flow  
846 models. *Geofluids*, No. 10, 94-113.

847 Martel, S. J. & Langley, J. S. 2006. Propagation of normal faults to the surface in basalt, Koa'e  
848 fault system, Hawaii. *Journal of Structural Geology*, 28, 2123-2143.

849 Michie, E. a. H., Haines, T. J., Healy, D., Neilson, J. E., Timms, N. E. & Wibberley, C. a. J.  
850 2014. Influence of carbonate facies on fault zone architecture. *Journal of Structural Geology*,  
851 65, 82-99.

852 Morley, C. K., Nelson, R. A., Patton, T. I. & Munn, S. G. 1990. Transfer zones in the East Africa  
853 Rift System and their relevance to hydrocarbon exploration in rifts. *The American Association*  
854 *of Petroleum Geologists Bulletin*, 74, 1234-1253.

855 Nahm, A. L., & Kattenhorn, S. A. 2015. A unified nomenclature for tectonic structures on the  
856 surface of Enceladus. *Icarus*, 258, 67-81.

857 Nahm, A. L. & Schultz, R. A. 2015. Rupes Recta and the geological history of the Mare Nubium  
858 region of the Moon: insights from forward mechanical modelling of the 'Straight Wall'.  
859 *Geological Society, London, Special Publications*, 401, 377-394.

860 Neal, C. A. & Lockwood, J. P. 2003. Geologic map of the summit region of Kilauea volcano,  
861 Hawaii. *USGS Geologic Investigation Series*, I-2759.

862 Nixon, C. W., Sanderson, D. J., Dee, S. J., Bull, J. M., Humphreys, R. J. & Swanson, M. H.  
863 2014. Fault interactions and reactivation within a normal-fault network at Milne Point,  
864 Alaska. *The American Association of Petroleum Geologists Bulletin*, 98, 2081-2107.

865 Opheim, J. A. & Gudmundsson, A. 1989. Formation and geometry of fractures, and related  
866 volcanism, of the Krafla fissure swarm, northeast Iceland. *Geological Society of America*  
867 *Bulletin*, 101, 1608-1622.

868 Owen, S., Segall, P., Lisowski, M., Miklius, A., Denlinger, R. P. & Sako, M. 2000. Rapid  
869 deformation of Kilauea Volcano: Global Positioning System measurements between 1990 and  
870 1996. *Journal of Geophysical Research*, 105, 18983.

871 Peacock, D. C. P. & Parfitt, E. A. 2002. Active relay ramps and normal fault propagation on  
872 Kilauea Volcano, Hawaii. *Journal of Structural Geology*, 24, 729-742.

873 Peacock, D. C. P. & Sanderson, D. J. 1991. Displacements, segment linkage and relay ramps in  
874 normal fault zones. *Journal of Structural Geology*, 13, 721-733.

875 Peacock, D. C. P. 2002. Propagation, interaction and linkage in normal fault systems. *Earth*  
876 *Science Reviews*, 58, 121-142.

877 Planke, S., Alvestad, E. & Eldhom, O. 1999. Seismic characteristics of basaltic extrusive and  
878 intrusive rocks. *The Leading Edge*, 342-348.

879 Plattner, C., Amelung, F., Baker, S., Govers, R. & Poland, M. 2013. The role of viscous magma  
880 mush spreading in volcanic flank motion at Kīlauea Volcano, Hawai‘i. *Journal of Geophysical*  
881 *Research: Solid Earth*, 118, 2474-2487.

882 Podolsky, D. M. W. & Roberts, G. P. 2008. Growth of the volcano-flank Koa’e fault system,  
883 Hawaii. *Journal of Structural Geology*, 30, 1254-1263.

884 Poland, M. P., Miklius, A., Sutton, A. J. & Thornber, C. R. 2012. A mantle-driven surge in magma  
885 supply to Kilauea Volcano during 2003-2007. *Nature Geoscience*, 5, 295-300.

886 Poland, M.P., Miklius, A., and Montgomery-Brown, E.K., 2014, Magma supply, storage, and  
887 transport at shield-stage Hawai‘ian volcanoes, *in* Poland, M.P., Takahashi, T.J., and

888 Landowski, C.M., eds., Characteristics of Hawai‘ian volcanoes: U.S. Geological Survey  
 889 Professional Paper 1801, p. 179–234.  
 890 Roman, D. C. & Gardine, M. D. 2013. Seismological evidence for long-term and rapidly  
 891 accelerating magma pressurization preceding the 2009 eruption of Redoubt Volcano, Alaska.  
 892 *Earth and Planetary Science Letters*, 371-372, 226-234.  
 893 Rowland, J. V., Baker, E., Ebinger, C. J., Keir, D., Kidane, T., Biggs, J., Hayward, N. & Wright,  
 894 T. J. 2007. Fault growth at a nascent slow-spreading ridge: 2005 Dabbahu rifting episode,  
 895 Afar. *Geophysical Journal International*, 171, 1226-1246.  
 896 Rubin, A. M. 1992. Dike-induced faulting and graben subsidence in volcanic rift zones. *Journal*  
 897 *of Geophysical Research: Solid Earth*, 97, 1839-1858.  
 898 Sæmundsson, K. 1974. Evolution of the axial rifting zone in northern Iceland and the Tjörnes  
 899 Fracture Zone. *Geological Society of America Bulletin*, 85, 495-504.  
 900 Schöpfer, M. P. J., Childs, C. & Walsh, J. J. 2006. Localisation of normal faults in multilayer  
 901 sequences. *Journal of Structural Geology*, 28, 816-833.  
 902 Schultz, R. A., Hauber, E., Kattenhorn, S. A., Okubo, C. H., & Watters, T. R. 2010.  
 903 Interpretation and analysis of planetary structures. *Journal of Structural Geology*, 32(6), 855-  
 904 875.  
 905 Seebeck, H., Nicol, A., Walsh, J. J., Childs, C., Beetham, R. D. & Pettinga, J. 2014. Fluid flow in  
 906 fault zones from an active rift. *Journal of Structural Geology*, 62, 52-64.  
 907 Segall, P. & Pollard, D. D. 1980. Mechanics of discontinuous faults. *Journal of Geophysical*  
 908 *Research*, 85, 4337-4350.

909 Sharp, I., Gawthorpe, R. L., Armstrong, B. & Underhill, J. R. 2000. Propagation history and  
 910 passive rotation of mesoscale normal faults: implications for syn-rift stratigraphic  
 911 development. *Basin Research*, 12, 285-305.

912 Soule, S. A., Escartin, J. & Fornari, D. J. 2009. A record of eruption and intrusion at a fast  
 913 spreading ridge axis: Axial summit trough of the East Pacific Rise at 9-10°N. *Geochemistry,*  
 914 *Geophysics, Geosystems*, 10.

915 Swanson, D. A., Duffield, W. A. & Fiske, R. S. 1976. Displacement of the south flank of Kilauea  
 916 Volcano: the result of forceful intrusion of magma into the rift zones. *US Geological Survey*  
 917 *Professional Paper*, 963.

918 Tanaka, K., Rodriguez, J., Skinnerjr, J., Bourke, M., Fortezzo, C., Herkenhoff, K., Kolb, E. &  
 919 Okubo, C. 2008. North polar region of Mars: Advances in stratigraphy, structure, and  
 920 erosional modification. *Icarus*, 196, 318-358.

921 Tentler, T. & Acocella, V. 2010. How does the initial configuration of oceanic ridge segments  
 922 affect their interaction? Insights from analogue models. *Journal of Geophysical Research*, 115,  
 923 1-16.

924 Toda, S., Stein, R. S. & Sagiya, T. 2002. Evidence from AD 2000 Izu islands earthquake swarm  
 925 that stressing rate governs seismicity. *Nature*, 419.

926 Tryggvason, E. 1984. Widening of the Krafla fissure swarm during the 1975-1981 volcano-  
 927 tectonic episode. *Bulletin of Volcanology*, 47-1, 47-69.

928 Tryggvason, E. 1986. Multiple magma reservoirs in a rift-zone volcano - ground deformation and  
 929 magma transport during the September 1984 eruption of Krafla, Iceland. *Journal of*  
 930 *Volcanology and Geothermal Research*, 28, 1-44.

931 Van Gent, H. W., Holland, M., Urai, J. L., & Loosveld, R. (2010). Evolution of fault zones in  
 932 carbonates with mechanical stratigraphy—Insights from scale models using layered cohesive  
 933 powder. *Journal of Structural Geology*, 32(9), 1375-1391.

934 Vaz, D. A., Spagnuolo, M. G., & Silvestro, S. (2014). Morphometric and geometric  
 935 characterization of normal faults on Mars. *Earth and Planetary Science Letters*, 401, 83-94.

936 Villemin, T. & Bergerat, F. 2013. From surface fault traces to a fault growth model: The Vogar  
 937 Fissure Swarm of the Reykjanes Peninsula, Southwest Iceland. *Journal of Structural Geology*,  
 938 51, 38-51.

939 Walker, R. J., Holdsworth, R. E., Imber, J. & Ellis, D. 2012. Fault-zone evolution in layered  
 940 basalt sequences: A case study from the Faroe Islands, NE Atlantic margin. *Geological*  
 941 *Society of America Bulletin*, 124, 1382-1393.

942 Walker, R. J., Holdsworth, R. E., Imber, J., Faulkner, D. R. & Armitage, P. J. 2013. Fault zone  
 943 architecture and fluid flow in interlayered basaltic volcanoclastic-crystalline sequences.  
 944 *Journal of Structural Geology*, 51, 92-104.

945 Walsh, J. J., Bailey, W. R., Childs, C., Nicol, A. & Bonson, C. G. 2003. Formation of segmented  
 946 normal faults: a 3D perspective. *Journal of Structural Geology*, 25, 1251-1262.

947 Wauthier, C., Roman, D. C. & Poland, M. P. 2016. Joint analysis of geodetic and earthquake  
 948 fault-plane solution data to constrain magmatic sources: A case study from Kīlauea Volcano.  
 949 *Earth and Planetary Science Letters*, 455, 38-48.

950 Wright, T. J., Sigmundsson, F., Pagli, C., Belachew, M., Hamling, I. J., Brandsdottir, B., Keir, A.,  
 951 Pedersen, R., Ayele, A., Ebinger, C., Einarsson, P., Lewi, E. & Calais, E. 2012. Geophysical  
 952 constraints on the dynamics of spreading centres from rifting episodes on lands. *Nature*  
 953 *Geoscience*, 5, 242-250.

954 Wright, T. L. & Klein, F. W. 2006. Deep magma transport at Kilauea volcano, Hawaii. *Lithos*, 87,  
955 50-79.  
956

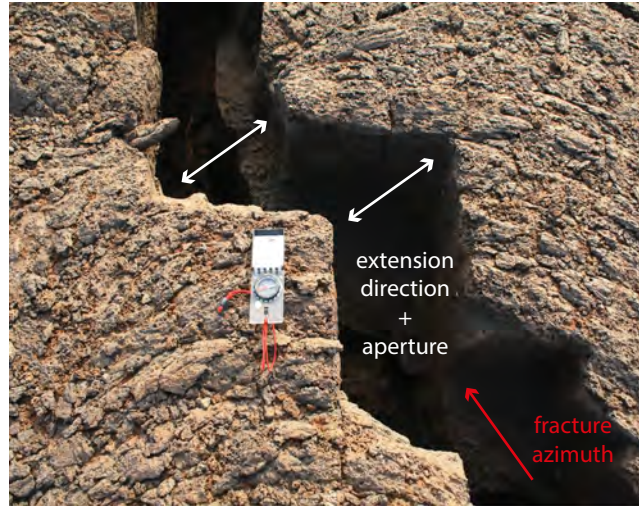


Figure 1. Measurement of fracture geometry and kinematics: extension-mode opening across pre-existing cooling joint surfaces allows the traditional measurement of opening direction, aperture, azimuth and vertical offset (where present).



Figure 2  
W: 121 mm  
H: 191.5 mm  
(double column width)

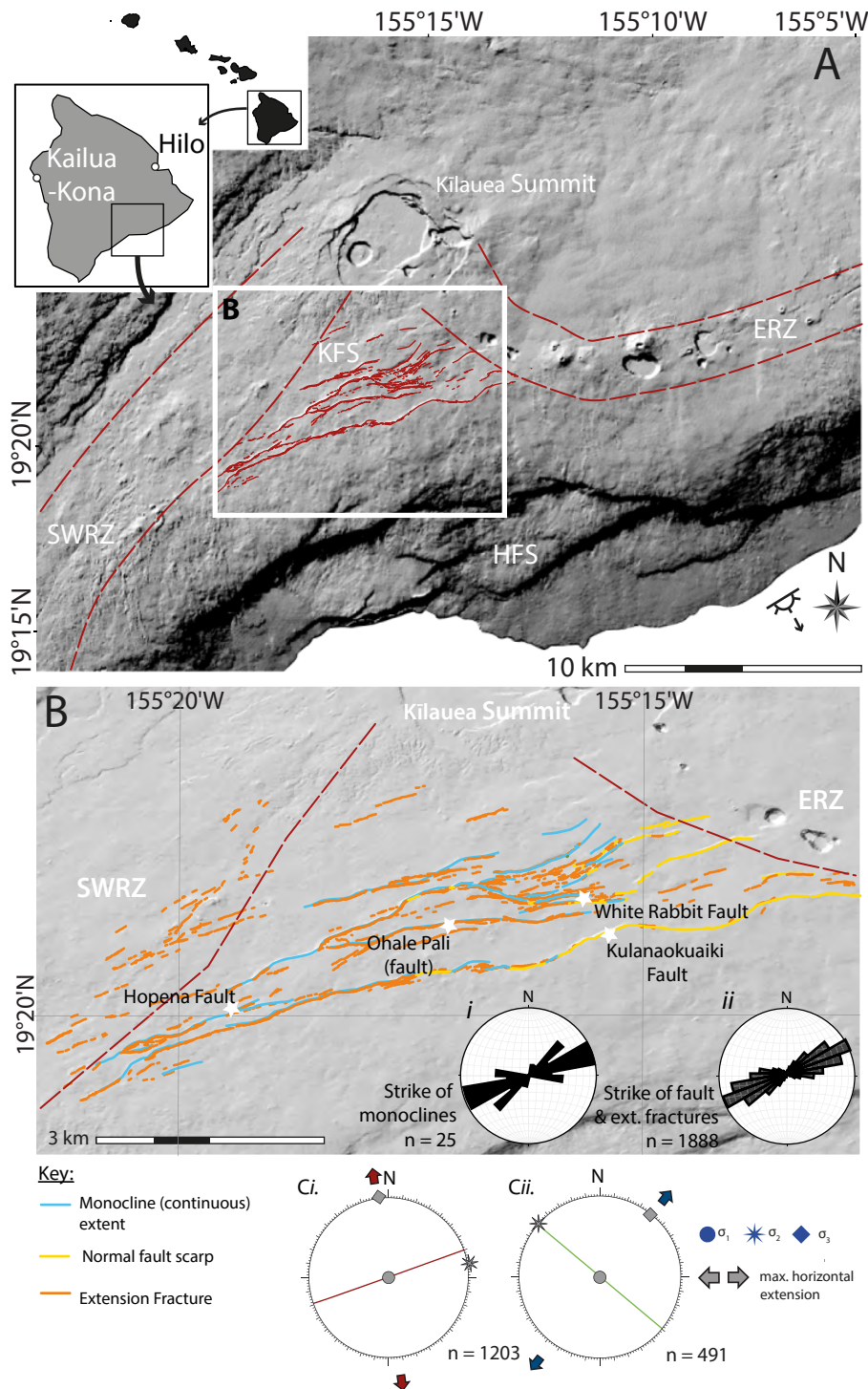


Figure 2. A. Simplified structural elements map of Kilauea Volcano: Koa'e fault system (KFS); ERZ: East Rift Zone; SWRZ: Southwest Rift Zone; HFS: Hilina Fault System. Inset shows relative position of A, on the south coast of Hawai'i. B. Map of extensional structures in the Koa'e fault system: (1) surface-breaking normal faults (yellow lines); (2) extension fracture networks (orange lines); and (3) monoclinical folds with lengths >150 m (blue lines). B.i. Rose diagram highlights the strike direction of monoclines in the Koa'e fault system. B.ii. Rose diagram highlights the strike direction of 1888 mapped fracture and faults in the Koa'e fault system. C. Lower hemisphere stereographic projections showing the average strike of fault/fractures and calculated maximum horizontal extension directions for the two dominant orientations: i) ENE-WSW striking (ERZ-parallel) structures, accommodating NNW-SSE extension; ii) NW-SE striking (ERZ-oblique) structures accommodating NE-SW extension.

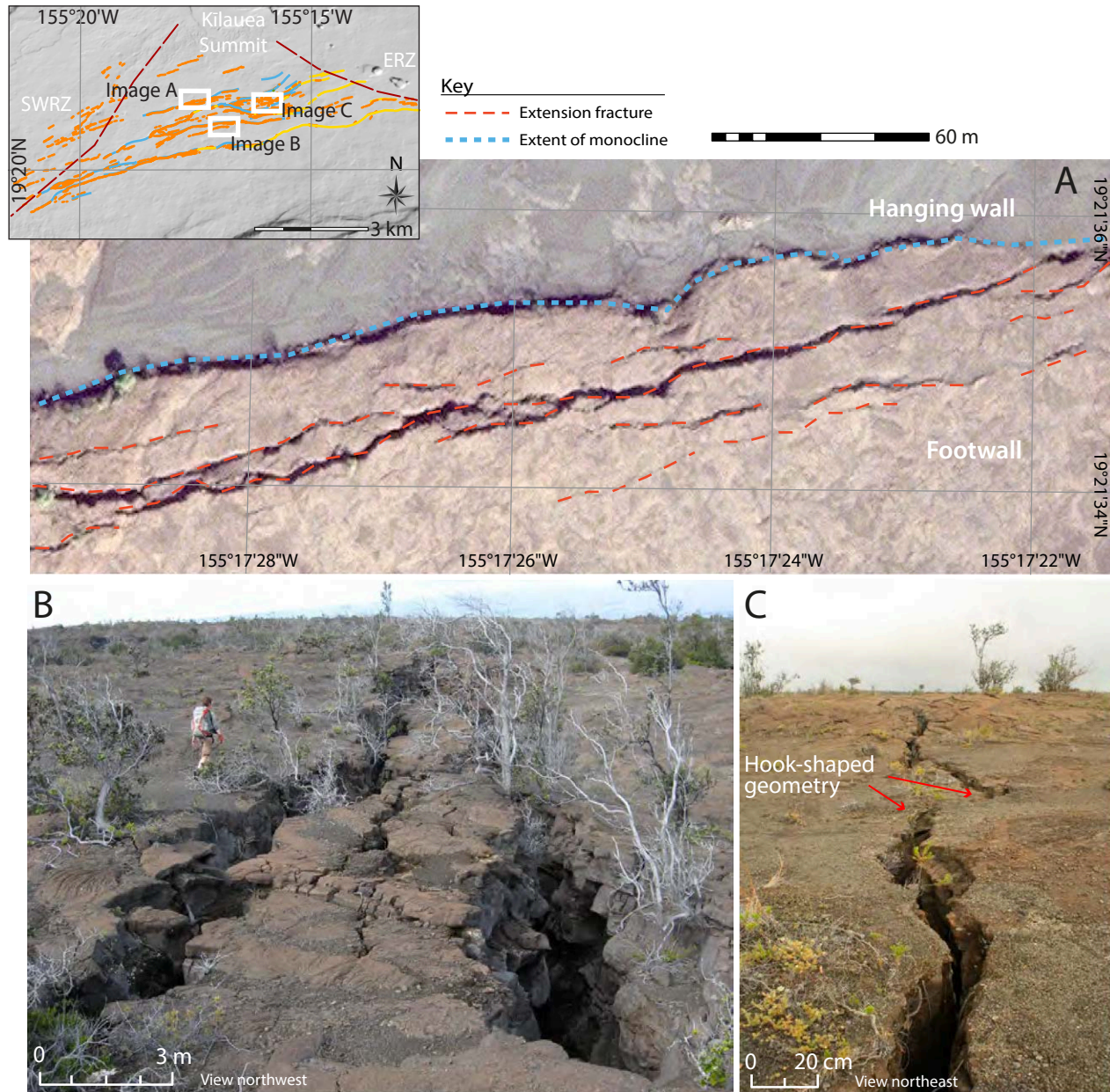


Figure 3. Scaling and location of extension fracture networks. A. At the 100's of metre-scale, fracture zones are predominantly located in the footwall of faults and along the upper limb of monoclines. Zones range from 30-50 m in width and extend for >1 km. Base image: aerial World-View 2 satellite image (0.5 m resolution). Inset map indicates image locations for parts A, B and C. B. At the 10's of metre-scale fractures show stepped geometries and apertures of up to ~4 m. C. At the cm-scale, fractures also demonstrate stepping trace geometries and "hook-shaped" tip geometries in the vicinity of neighbouring fracture tips. At these scales, fractures are also observed in otherwise undeformed (i.e. not folded, non-faulted) regions of the fault system.



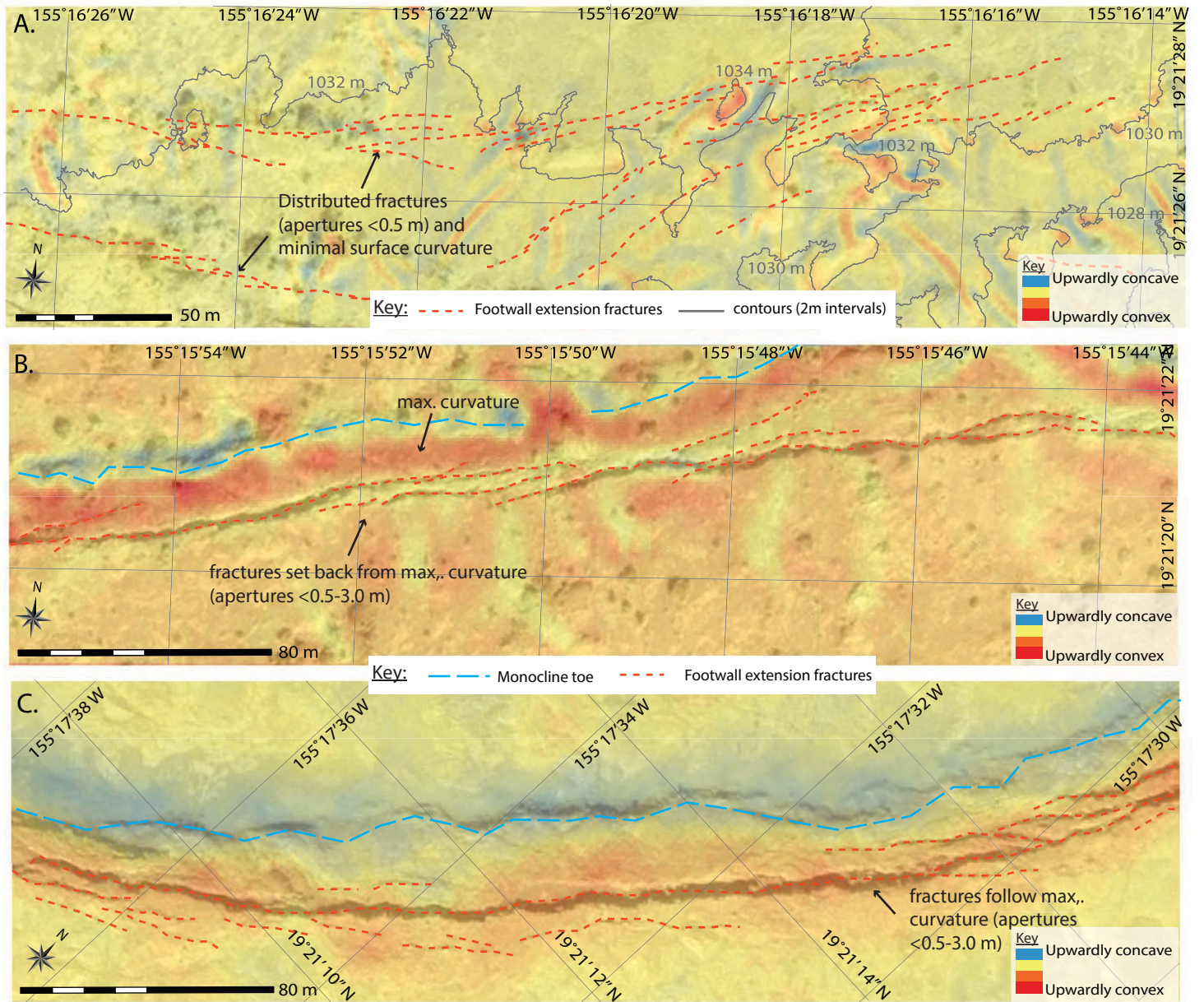


Figure 4. Maps of 3D surface curvature derived from aerial LiDAR datasets and examples of extension fracture distribution in the Koa'e fault system. A positive curvature (warm colours) indicates the surface is upwardly convex; a negative curvature (cold colours) indicates the surface is upwardly concave. A. Fracture networks are present in areas of the fault system where there is no topographic expression of fault slip (i.e. monoclines, or fault scarps). Anomalous regions of curvature are associated with tumuli and the general morphology of the lava field. B. Fracture networks occur along the upper limb of monoclines where they are not spatially associated with regions of maximum curvature across monoclines. C. Fracture networks show a strong spatial relationship with regions of maximum curvature across monoclines.



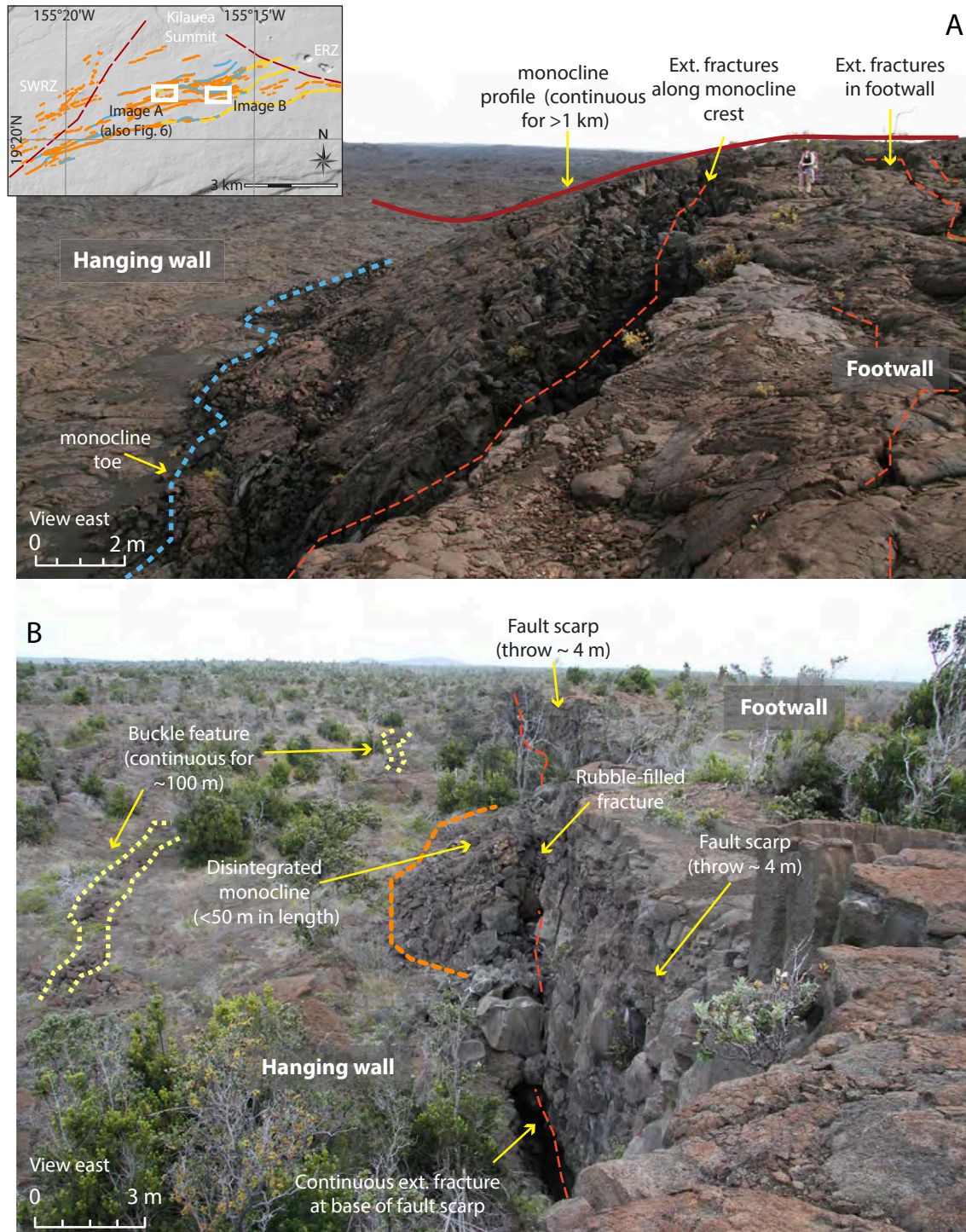


Figure 5. Examples of monocline type in the Koa'e fault system. Inset map indicates image locations for parts A and B. A. Laterally continuous monoclines with fold limbs that dip gently and vary from a 2 m to ~ 10 m in amplitude. Zones of fractures are found along the upper limbs and rubbly toes at the base. Crests can be traced for over 1 km. B. Laterally discontinuous monoclines form densely fractured, often disintegrated blocks in the hanging wall of faults. Lengths vary from 10 m to 150 m and amplitudes from 2 m to 15 m. Solid red line in part A highlights monocline profile. Dashed blue lines: extent of continuous monocline; dashed orange line indicates extent of discontinuous monocline; dashed red lines: continuous open fracture; dashed yellow lines: extent of hanging wall buckles.



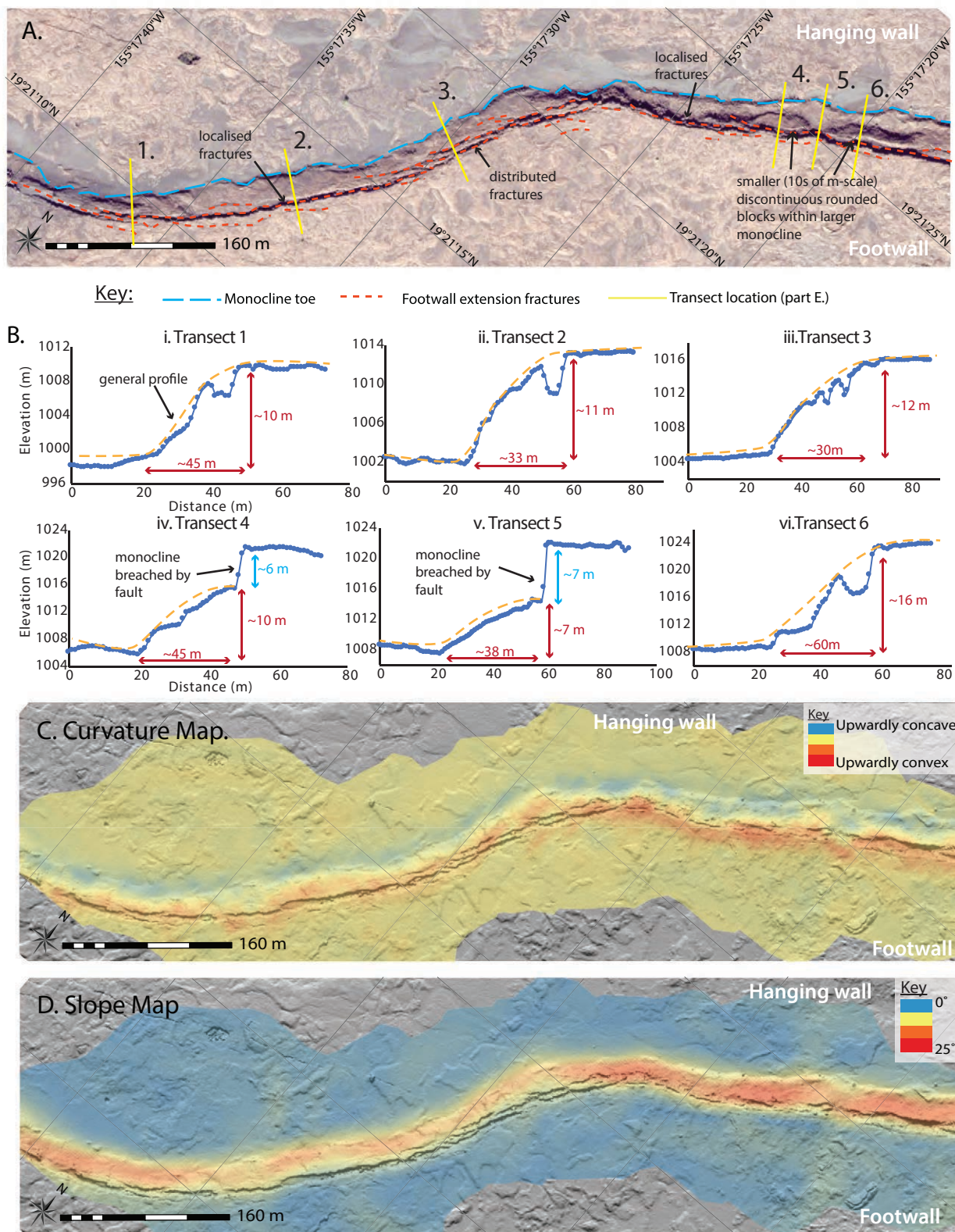


Figure 6. A. Map view of the continuous monocline shown in Figure 5, showing the distribution of extension fractures along the upper limb (dotted red lines). For location, please refer to the inset map for Figure 5. B. Cross-sections across the monocline in part A. Transect locations are shown in part A. Transects 1-3 and 6 show steep, rounded monoclines with extension fractures along the region of maximum curvature. Transects 4 and 5 show a region of the monocline that has been breached by fault segments. The extent of this breaching is spatially limited. C. A map highlighting changes in 3D surface curvature across the monocline in part A. D. A slope map across the monocline in part A. Slope angles for the monocline limb range from ~12-25° with these values varying along-strike. Base image in A is an aerial World-View 2 satellite image (0.5 m resolution). Terrain data in parts C and D are derived from aerial LiDAR dataset (0.5 m resolution) provided by OpenTopography and generated in ArcGIS® software by Esri.



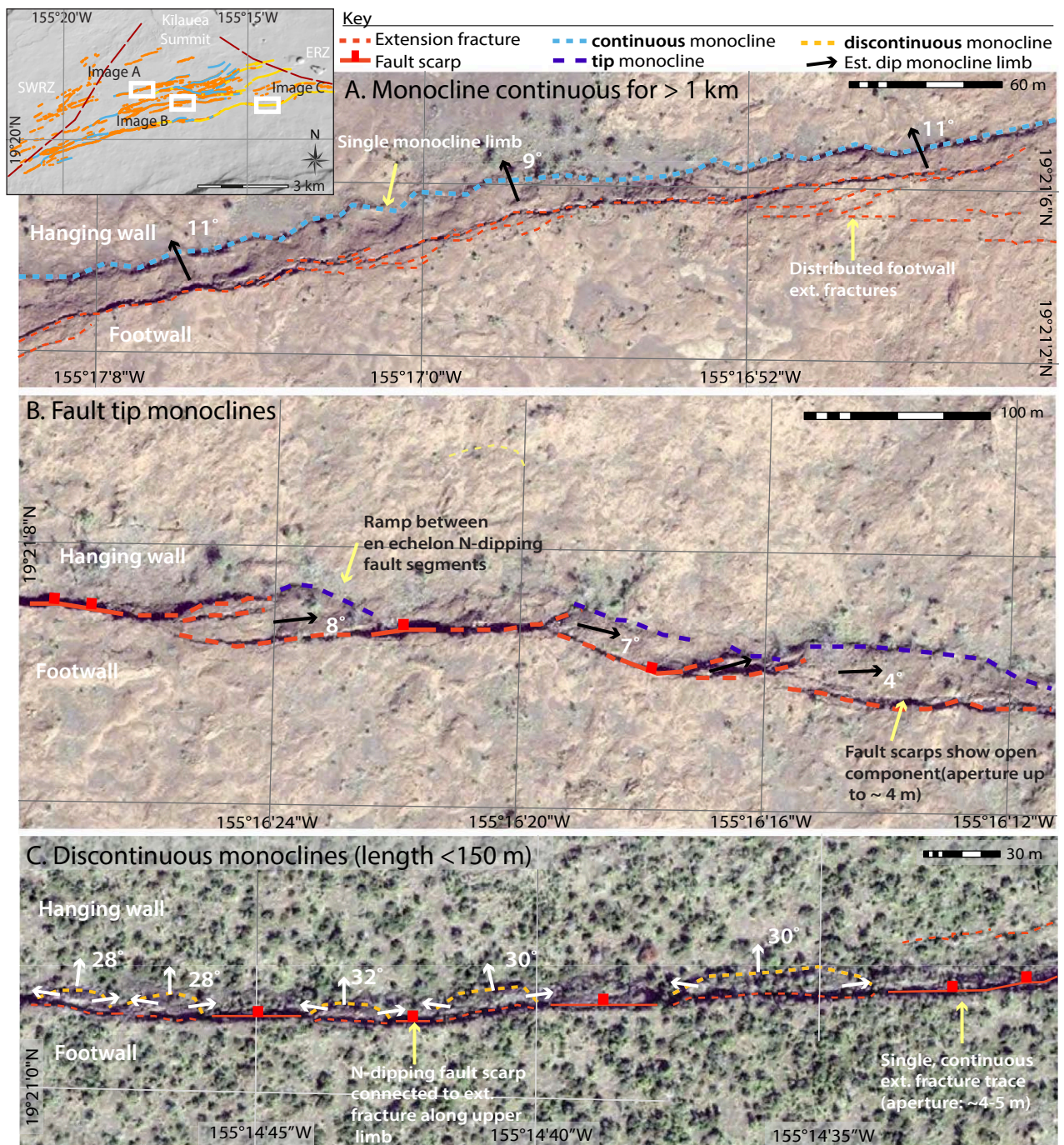


Figure 7. Map view of monocline types. A. Continuous monocline with a network of extension fractures along the upper limb. Limbs dip towards the north at  $\sim 10^\circ$ . Breached continuous monoclines are observed, but less commonly than unbreached. B. Fault tip monoclines between en echelon segments along the Ohale Fault. Tip monoclines dip parallel to the bounding segments by  $\sim 10^\circ$ . C. Discontinuous monocline blocks (dotted, yellow lines), isolated between normal fault segments (heavy red line), connected by collinear extension fractures (dotted red line) along the upper limb to form continuous open fractures that decouple the monocline from the footwall. These monoclines dip more steeply ( $\sim 30^\circ$ ) from a central amplitude maxima, to zero at the lateral edges. Breached discontinuous monoclines have not been observed. Base images: World-View 2 satellite image (0.5 m resolution).



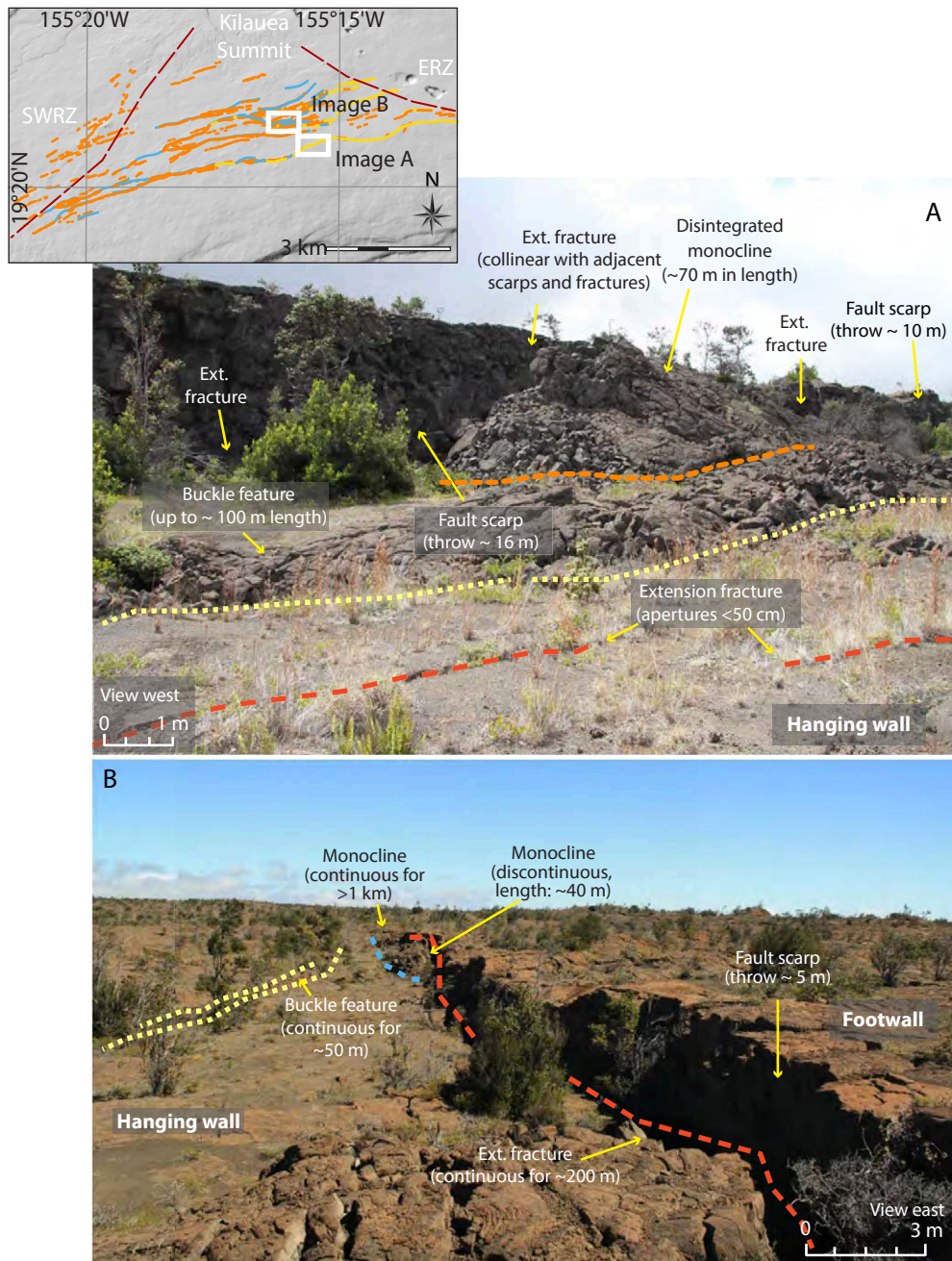


Figure 8. Examples of surface-breaking normal fault segments in the Koa'e fault system. Inset map indicates location for images in Part A and B. A. The largest vertical offsets (up to ~15m) and greatest proportion of fault scarps are found on the Kulanaokuaiki ("Shaking Spine") fault. B. Where present, scarps show a significant component of horizontal opening and offset planar footwall and hanging wall ground surfaces. Also present along many (but not all) faults in the Koa'e fault system are hanging wall buckles that occur ahead of both fault scarps and monoclinical structures. Dashed orange line: extent of discontinuous monocline; dashed blue lines: extent of continuous monocline; dashed red lines: continuous open fracture; dashed yellow lines: extent of hanging wall buckles.

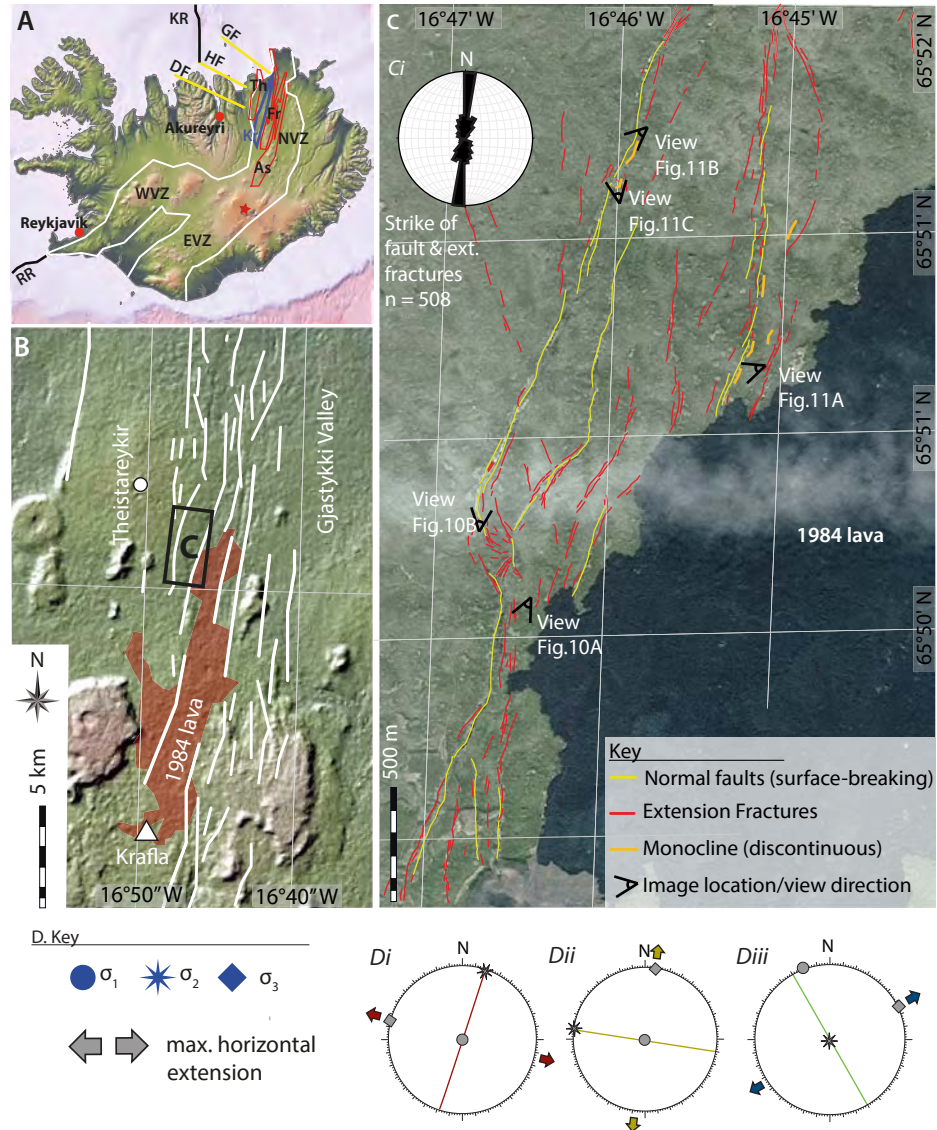


Figure 9. A. Map of Iceland highlighting the major tectonic elements: Reykjanes Ridge (RR); the Kolbeinsey Ridge (KR); West Volcanic Zone (WVZ); East Volcanic Zone (EVZ); Neo-Volcanic Zone (NVZ: the axial rift zone); Askja volcanic centre (As); Fremri-Namur volcanic centre (Fr); Krafla volcanic centre, (highlighted blue; Kr); Theistareykir volcanic centre (Th); the Dalvík lineament (DF), the Husavík-Flatey Fault (HF) and the Grimsey lineament (GF). B. Location of study area in the Gjastykki Valley within the Krafla fissure swarm. C. Mapped faults and extension/oblique-extensional fractures in the study area. Image locations and view directions in Figures 10 and 11 are indicated. Ci. Rose diagram highlights the strike of normal faults and fractures in the Krafla fissure swarm. D. Lower hemisphere stereographic projections showing the average strike of fault/fractures and calculated maximum horizontal extension directions for the three dominant orientations: i) NNE-SSW striking faults and fractures, accommodating WNW-ESE extension; ii) WNW-ESE striking fractures, accommodating NNE-SSW extension; iii) NW-SE striking faults and fractures, accommodating ENE-WSW extension.



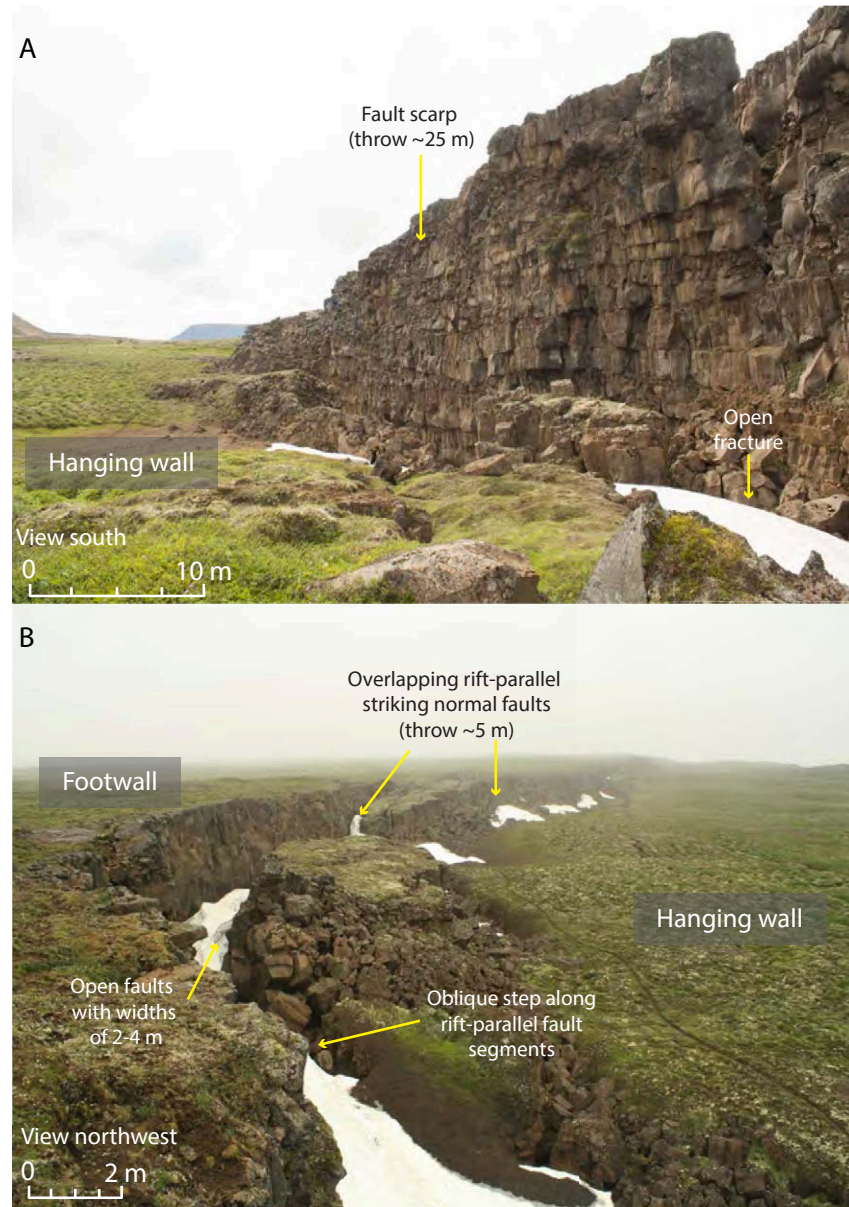


Figure 10. A. Examples of surface-breaking normal fault segments in the Gjastykki area of the Krafla fissure swarm. A. Subvertical normal faults demonstrate throws of up to 25-30 m and offset planar footwall and hanging wall surfaces. B. Rift faults show prominent horizontal openings of 2-4 m and overlapping geometries with obliquely-oriented linking segments. Inset map indicates the location of images in part A and B.

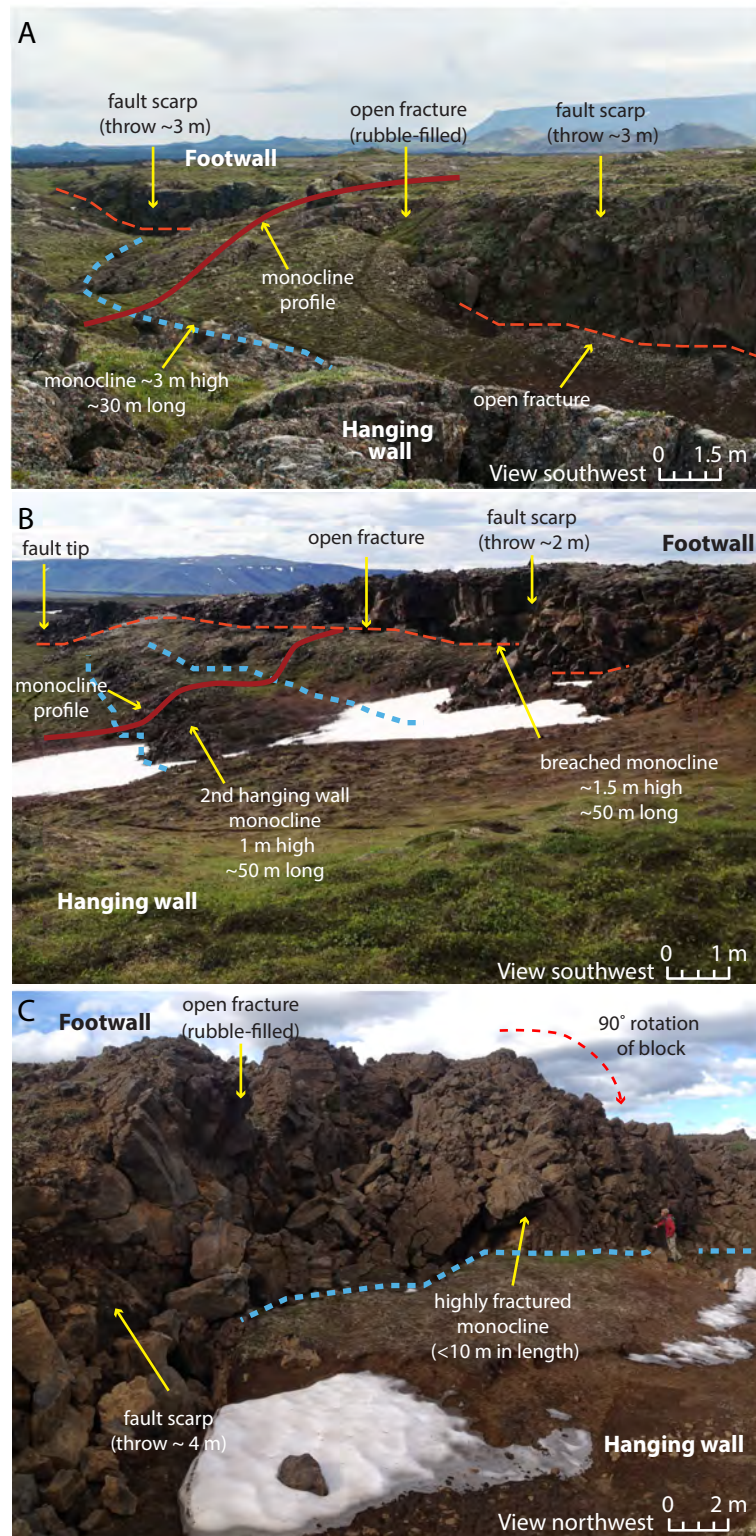


Figure 11. Examples of monoclines in the Krafla fissure swarm. A. Monoclines show amplitudes of up to ~3 m with open fractures along their upper limbs that are co-linear with fault segments on either side. B. Breached monocline observed in the hangingwall of a surface-breaking normal fault with vertical offset of up 2-3 m. Along the fault in the image, an additional monocline has developed further into the hangingwall. C. Monoclines can also be strongly fragmented and show steep rotations. In all examples, their lateral extent is <50 m.



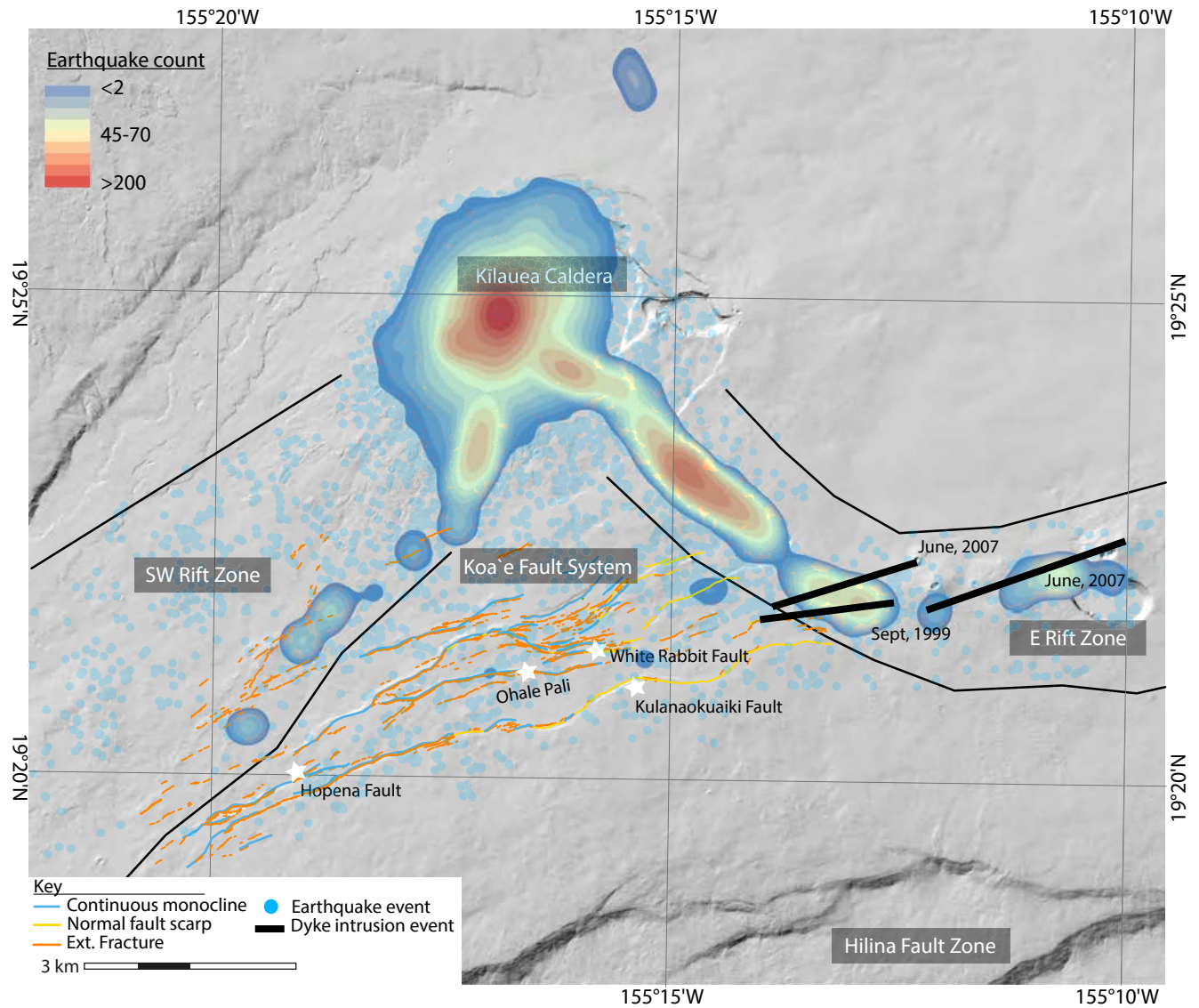
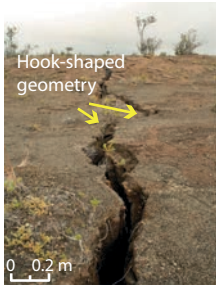
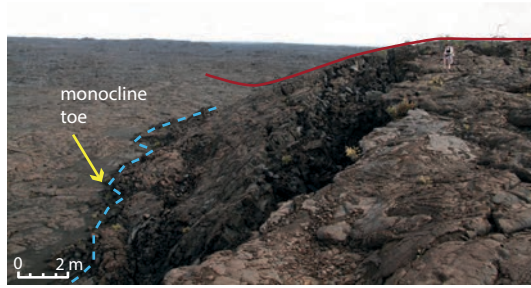


Figure 12. Distribution of surface-breaking normal faults and monoclinical folds across the Koa'e fault system. Blue circles represent focal mechanisms in the summit, upper ERZ and upper SWRZ regions of Kilauea Volcano from the period 1986-2009. Contours highlight the density of events based on approx. 3000 focal mechanisms recorded in this region. Earthquake data reproduced from Lin and Okubo, 2016. ~90% of focal mechanisms in the catalog are small earthquakes (96% <M2.5), from shallow depths (i.e. <13 km); half of the focal mechanisms come from 2-5 km depth. Dyke intrusion events taken from Baker and Amelung, 2015 and Cervelli et al., 2002.

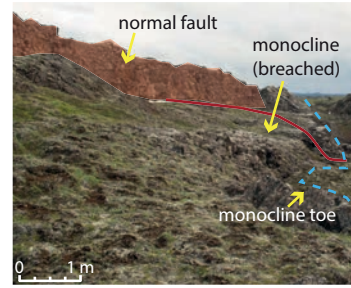
1) en-echelon extension fractures



2) continuous monocline



3) normal fault & breached monocline



4) normal fault & discontinuous monocline

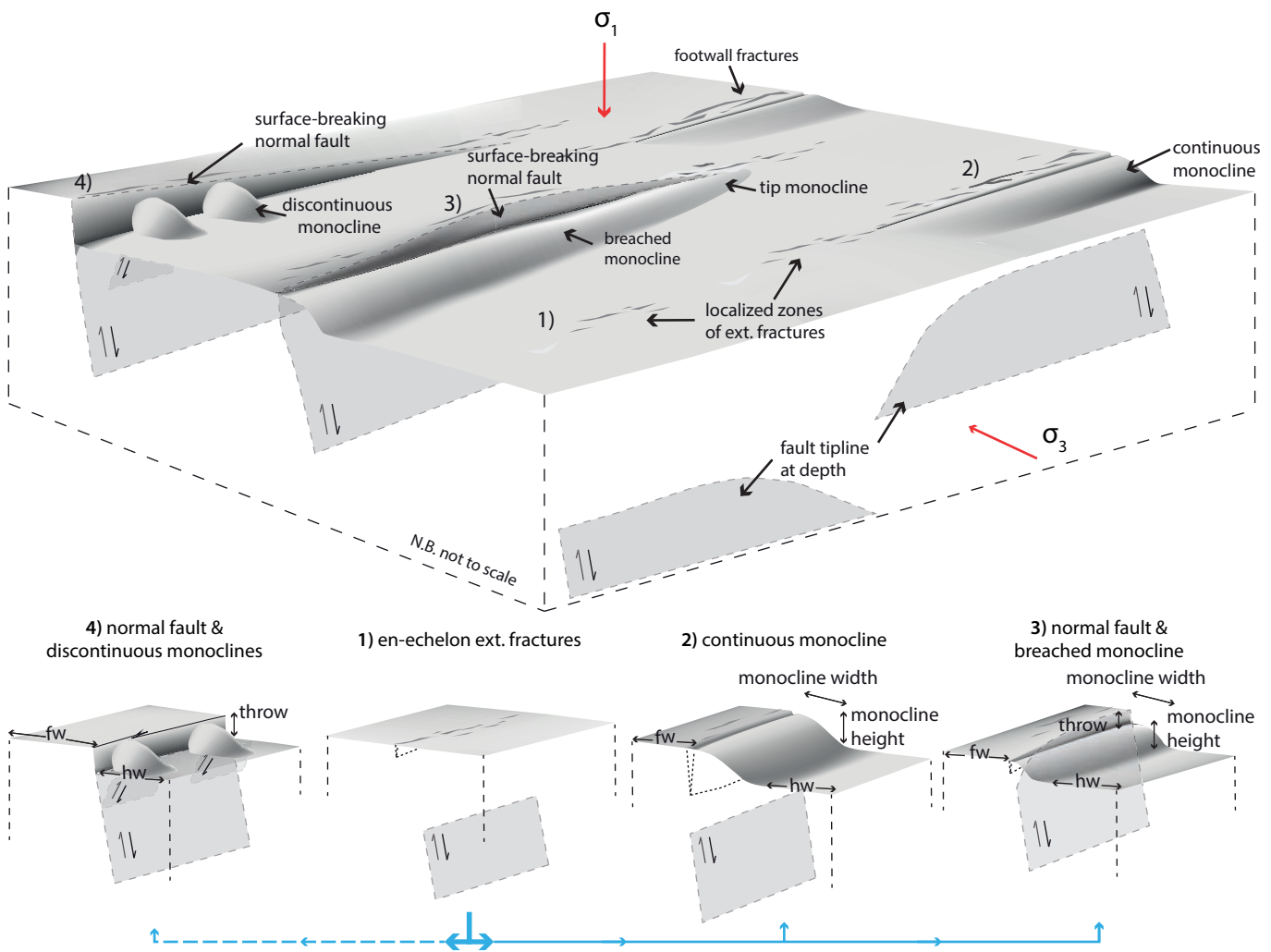
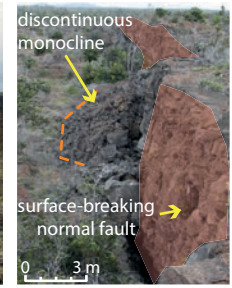


Figure 13. Conceptual model for growth faults in volcanic rift zones with spatially (and temporally) variable strain rates. Principal stress axes (red arrows) represent the regional stress state acting on the rift zone.

1. Precursory extension fractures localise in narrow zones at the free surface ahead of blind normal faults.
2. In regions of the rift zone where strain rates are low, faults remain at depth where they accumulate slip aseximally and gradually deform the free surface ahead of the tipline into monoclines.
3. In regions of the rift zone that experience episodically high strain rates, faults may spend protracted periods segmented at depth, followed by a rapid propagation phase that results in linkage with surface fractures and breaching of earlier formed monoclines at the free surface.
4. In regions of the rift zone where strain rates are high, normal faults propagate rapidly upwards through the sequence and link with downward propagating surface fractures, producing fault scarps. A lack of preserved monocline indicates strain rates have remained high since the last resurfacing event. Antithetic faults may develop from points of stress concentration, causing a rotation of the hanging wall block above them.